

DTIC FILE COPY

①

1990

Thesis/Dissertation

Storm Induced Changes of the Topside Ionosphere as
Deduced from Incoherent Scatter Radars

Kevin John Lunn

AFIT Student at: University of California Los Angeles

AFIT/CI/CIA - 90-106

AFIT/CI
Wright-Patterson AFB OH 45433

DTIC
ELECTE
OCT 24 1990
S B D

Approved for Public Release IAW AFR 190-1 -
Distribution Unlimited
ERNEST A. HAYGOOD, 1st Lt, USAF
Executive Officer, Civilian Institution Programs

AD-A227 899

UNIVERSITY OF CALIFORNIA

Los Angeles

Storm Induced Changes of the Topside Ionosphere
as Deduced from Incoherent Scatter Radars

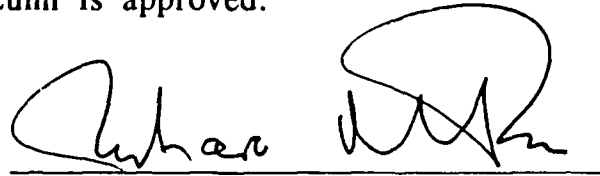
A thesis submitted in partial satisfaction of the
requirements for the degree Master of Science
in Atmospheric Science

by

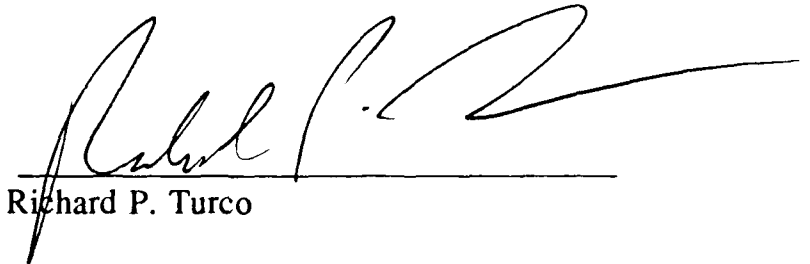
Kevin John Lunn

1990

The thesis of Kevin John Lunn is approved.



Richard M. Thorne



Richard P. Turco



S. V. Venkateswaran, Committee Chair

University of California, Los Angeles

1990

Accession For	
NTIS GRA&I	<input checked="checked" type="checkbox"/>
DTIC TAB	<input type="checkbox"/>
Unannounced	<input type="checkbox"/>
Justification	
By	
Distribution/	
Availability Codes	
Dist	Avail and/or Special
A-1	

To my son Kevin Jr.,
and the rest of my family and friends
who have helped me make it this far.

TABLE OF CONTENTS

	<u>PAGE</u>
LIST OF DIAGRAMS	vi
ACKNOWLEDGEMENTS	ix
ABSTRACT OF THESIS	xi
INTRODUCTION	1
CHAPTER 1 UPPER-ATMOSPHERIC PHYSICAL PROCESSES	5
Electron Density	5
Electron and Ion Temperatures	9
Neutral Winds at Ionospheric Heights	13
Figure Captions for Chapter One	16
CHAPTER 2 THE INCOHERENT SCATTER RADAR	20
Theory	20
Determination of Physical Parameters	24
Figure Captions for Chapter Two	29
CHAPTER 3 THE QUIET IONOSPHERE	31
Millstone Hill Electron Density	31
Millstone Hill Electron and Ion Temperatures	32
Arecibo Electron Density	33
Arecibo Electron and Ion Temperatures	35
Parallel Ion Velocities	36
Figure Captions for Chapter Three	38
CHAPTER 4 THE DISTURBED IONOSPHERE	49
Millstone Hill Electron Density	49
Millstone Hill Electron and Ion Temperatures	51
Arecibo Electron Density	52
Arecibo Electron and Ion Temperatures	54
Average Ionic Mass in the Topside Ionosphere	55
Parallel Ion Velocities	57
Global View of the Ionospheric Disturbance	60

Figure Captions for Chapter Four	<u>PAGE</u> 62
CHAPTER 5 ANTI-CORRELATED OSCILLATIONS OF PARALLEL AND PERPENDICULAR ION DRIFT VELOCITIES DURING A GEOMAGNETIC STORM	76
Three Possible Mechanisms	
Ion Drag	76
Polarization Electric Field	77
Diffusion Mechanism	77
Quiet Time Oscillations	79
Disturbed Time Oscillations	80
Figure Captions for Chapter Five	82
CHAPTER 6 CONCLUSIONS AND FUTURE WORK	90
REFERENCES	94

LIST OF FIGURES

Figure 1-1	Vertical distribution of electron density	p. 17
Figure 1-2	Global distribution of neutral temperature and wind pattern at 300 km	p. 18
Figure 1-3	Schematic view of heat input to high-latitude ionosphere and sketch of storm-time circulation	p. 19
Figure 2-1	The dependence of the power spectrum on the temperature ratio T_e/T_i	p. 30
Figure 2-2	Power spectrum response to various drift conditions	p. 30
Figure 3-1	Electron density contoured against height and time over Millstone Hill on 18 September 1984	p. 40
Figure 3-2	Electron and ion temperatures contoured against height and time over Millstone Hill on 18 September 1984	p. 41
Figure 3-3	Diurnal variation of electron and ion temperature over Millstone Hill at 300 km on 18 September 1984	p. 42
Figure 3-4	Energy Budget of the nocturnal ionosphere	p. 43
Figure 3-5	Electron density contoured against height and time over Arecibo on 17 October 1984	p. 44
Figure 3-6	Diurnal variation of antiparallel ion velocity, northward perpendicular ion drift, and height of maximum electron density over Arecibo on 18 September 1984	p. 45
Figure 3-7	Electron and ion temperatures contoured against height and time over Arecibo on 17 October 1984	p. 46

Figure 3-8 Diurnal variation of electron and ion temperature over Arecibo at 300 km on 17 October 1984	p. 47
Figure 3-9 Antiparallel ion velocities over Millstone Hill, Saint Santin, and Arecibo during quiet conditions	p. 48
Figure 4-1 AE index for 18-20 September 1984	p. 64
Figure 4-2 Electron density contoured against height and time over Millstone Hill on 19 September 1984	p. 65
Figure 4-3 Electron and ion temperatures contoured against height and time over Millstone Hill on 18 September 1984	p. 66
Figure 4-4 Diurnal variation of electron and ion temperature over Millstone Hill at 300 km on 19 September 1984	p. 67
Figure 4-5 Electron density contoured against height and time over Arecibo on 19 September 1984	p. 68
Figure 4-6 Maximum electron density over Arecibo on 18-19 September 1984	p. 69
Figure 4-7 Diurnal variation of antiparallel ion velocity, northward perpendicular ion drift, and height of maximum electron density over Arecibo on 19 September 1984	p. 70
Figure 4-8 Electron density contoured against height and time over Arecibo on 19 September 1984	p. 71
Figure 4-9 Diurnal variation of electron and ion temperature over Arecibo at 300 km on 19 September 1984	p. 72

Figure 4-10	Average ionic mass in the topside ionosphere over Millstone Hill and Arecibo for magnetically quiet and disturbed days	p. 73
Figure 4-11	Antiparallel ion velocities over Millstone Hill, Saint Santin, and Arecibo for geomagnetically disturbed conditions	p. 74
Figure 4-12	Global view of ionospheric disturbance	p. 75
Figure 5-1	Sketch of ion drag mechanism	p. 83
Figure 5-2	Sketch of polarization electric field mechanism	p. 83
Figure 5-3	Sketch of diffusion mechanism	p. 84
Figure 5-4	Height of F layer response to the three mechanisms	p. 84
Figure 5-5	Anti-correlation of ion velocity components and height of maximum density over Arecibo on 17 October 1984	p. 85
Figure 5-6	Anti-correlation of ion velocity components over Arecibo on 14 September 1983	p. 86
Figure 5-7	Anti-correlation of ion velocity components and height of maximum density over Arecibo on 19 September 1984	p. 87
Figure 5-8	Anti-correlation of ion velocity components over Arecibo on 2 November 1983	p. 88
Figure 5-9	Anti-correlation of ion velocity components over Saint Santin on 23 March 1983	p. 89

ACKNOWLEDGEMENTS

I'd like to thank Professor S.V. Venkateswaran (Venki) for his guidance, support, and friendship over the past two years. With his helpful comments and daily dose of encouragement, I was able to keep on track through many adversities.

I am grateful to Dr. Art Richmond and Dr. Barbara Emery for thier advice and for allowing me to use the the computer facilities at NCAR. I send thanks to Roy Barnes for the time he spent teaching me how to use his computer programs that enabled me to access the data in the Incoherent-Scatter Radar Data Base. While at NCAR, I met Dr. Geoff Crowley whom first got me interested in analyzing data from the Equinox Transition Study of September 1984. Since our initial meeting we have had many valuable conversations.

Without the daily help from the staff of the Atmospheric Sciences department, I wouldn't have been able to do all the necessary work. Thanks goes out to all my friends and fellow students, especially Delores, Doug, Tim, and Tim who helped me through the good and bad times.

A special thought goes to Kathy for putting up with me on a daily basis and helping me with everything. She made it possible for me to make it through this program.

I'm also grateful to the U.S. Air Force for the opportunity to do my graduate studies at UCLA.

This study made use of the NCAR Incoherent-Scatter Radar Data Base, which is supported by the National Science Foundation.

Thanks also goes to Dr. Christine Mazaudier for her helpful comments and for supplying figure 5-9. Delores Knipp provided figure 4-12 from the AMIE procedure. Under the consent agreement of the *Journal of Geophysical Research*, I extracted figure 3-4. Finally, figure 1-3(a) is non-copyright material from *An Initial Feasibility Study to Establish a Very High Latitude Incoherent Scatter Radar* (from the National Science Foundation) by P.M. Banks and J.V. Evans, 1 September 1979.

ABSTRACT OF THE THESIS

Storm Induced Changes of the Topside Ionosphere as Deduced from Incoherent Scatter Radars

by

Kevin John Lunn

Master of Science in Atmospheric Science

University of California, Los Angeles, 1989

Professor S. V. Venkateswaran, Chair

Incoherent scatter radar observations from Millstone Hill, Saint Santin, and Arecibo are used to illustrate changes of the topside ionosphere during a geomagnetic storm. These observations consist of electron density, electron and ion temperatures, and ion velocity components parallel and perpendicular to the magnetic field. These parameters can further describe changes in ion composition, electric fields, and neutral winds. Attention is given to a specific storm during the Equinox Transition Study (ETS) of September 1984. In order to isolate the storm effects in the topside ionosphere, a comparison will be made between a disturbed and quiet day. A novel result from this study is the finding of correlated oscillations between parallel and perpendicular ion velocity components which are apparently storm induced. Previously,

these oscillations have been observed primarily at night, but now it's noticed that during storm conditions there are prominent oscillations during the day.

Introduction

The storms that affect the topside ionosphere (that portion of the ionosphere above the F2 peak) are geomagnetic storms that originate from the sun. The sun transmits its disturbances to the earth's ionosphere through a complex solar-terrestrial system. The common link to both the sun and the earth is their magnetic fields through which the information is passed.

The sun is continuously emitting energy into space. This energy is either black-body radiation (sunlight), radiation in the form of X rays, extreme ultra viol (EUV), and ultra violet (UV); and an outflow of charged particles. These particles which have energies of less than 1 keV make up a plasma (an ionized gas made up of an equal number of negative and positive charged particles). This plasma makes up the outermost solar atmosphere (the corona). This flow of solar plasma into outer space is called the solar wind. The flow is produced by the pressure difference between the hot dense gas in the corona and the cold tenuous gas of interstellar space.

Since charged particles are "tied" to the magnetic field lines (through the Lorentz force), the outflow of particles also means an outflow of the sun's magnetic field. When this continual outflow of solar wind (plasma and magnetic field) runs into the earth's magnetic field, the earth's dipole magnetic field is distorted and confined into a cavity with a long tail in the anti-sunward direction. This cavity is called the magnetosphere.

The solar wind/magnetosphere system described is a static one. The strength of the solar wind is constantly changing in time and direction (magnetic field) due to variable source regions on the sun. When a large change in the solar wind occurs, the magnetosphere is either compressed or decompressed. These sudden changes are seen on the earth as changes in the geomagnetic field (which are traditionally known as geomagnetic storms).

Solar wind interaction with the earth's magnetic field can drive electric currents along magnetic field lines. These so called field aligned currents close through the high-latitude ionosphere (auroral oval). Frictional dissipation of these currents in the ionosphere along with particle precipitation from magnetospheric processes into the auroral oval add large amounts of energy to relatively small areas of the upper-atmosphere.

Since the ionosphere is a region of the atmosphere where both neutral and charged particles occur, the geomagnetic storm causes electrodynamical changes in the charged particles and hydrodynamical changes in the neutral gas. The charged constituents of the ionosphere constitutes only about 1% of the total pressure at the F2 peak where plasma density is greatest. Heat that is given to charged particles due to Joule dissipation and particle bombardment is rapidly shared with the neutrals because of collisions. This heat input to the neutral atmosphere causes neutral air motions that can in turn control the ionized

portion as well. The electrodynamical and hydrodynamical changes are strongly coupled (Blanc and Richmond, 1980). Since the neutral atmosphere dominates this region, the heat input causes a storm-induced circulation in the upper-atmosphere (thermosphere).

Starting in the late 1950's and early 1960's these storm-induced changes could be remotely sensed by ground based Incoherent scatter radars. These radars are able to measure ionospheric parameters such as electron density, electron and ion temperature, and ion velocity components to name a few.

In this thesis we illustrate changes in the topside ionosphere during a geomagnetic storm. Up to three radars will be used to give a description of the mid-latitude topside ionosphere. The radars are located at Millstone Hill, Massachusetts (42.6°N , 71.5°W), Saint Santin, France (47.4°N , 2.2°E), and Arecibo, Puerto Rico (18.3°N , 66.7°W). Data from a storm that occurred on 19 September 1984 is available and is known as the 1984 Equinox Transition Study (ETS) case (17-24 September 1984). There were two geomagnetically quiet days preceding the storm day. The 18th of September is used as a control day for the radar at Millstone Hill. An equipment malfunction at Arecibo on 18 September caused a large data gap. Another quiet day (17 October 1984), that is still considered in the equinox period, is used for a control day at Arecibo. The Saint Santin radar also has numerous data gaps and a lower resolution in its observations which make it

undesirable for most of the ionospheric parameters. However, the Saint Santin radar does measure ion velocity components frequently enough to give good results.

A brief review of some necessary upper-atmospheric processes is given in chapter one. This includes production and loss processes of electron density, sources and sinks for plasma temperatures, and a basic picture for understanding the thermospheric circulation pattern. In chapter two there's a review of the incoherent scatter radar theory and determination of ionospheric parameters. The storm effects of the topside ionosphere are illustrated by comparing and contrasting the quiet and disturbed time plots of ionospheric variables in chapters three and four. Finally in chapter five a storm-induced anti-correlation between ion velocity components is discussed.

Chapter 1 Upper-Atmospheric Physical Processes

In order to study quiet and disturbed variations of ionospheric parameters, some basic physical processes of the upper-atmosphere need to be briefly reviewed.

1-1 Electron Density

The upper-atmosphere is ionized by radiation from the sun and by energetic particle precipitation. The ionized portion is composed of electrons and ions and is called the ionosphere. The ionosphere can be divided into two major zones: a high-latitude region which is dominated by energetic particle precipitation and a mid and low-latitude region that is dominated by solar radiation. There are also several distinct layers of charged particles that exist (figure 1-1).

The lowest region of the ionosphere is named the D region. It extends from 60-90 km, and has electron densities of 10^8 - 10^{10} m^{-3} during the day. The main source of ionization in the D region is X-radiation which ionizes oxygen and nitrogen. Lyman-alpha radiation from the sun is also an important source for nitric oxide ionization.

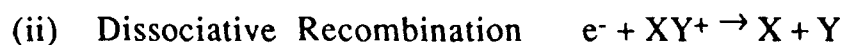
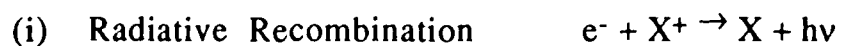
The next region is called the E region and extends from 90-140 km. Soft solar X-rays produce the ionization here and the average day time electron density is about 10^{11} m^{-3} .

The F layer lies on top of the E layer and is divided into the F1 layer from 140-200 km and the F2 layer above 200 km. The ionosphere has a maximum electron density of about 10^{12}

per m^{-3} and this occurs at the F2 peak. The ionization in the F region is the result of EUV radiation from 20-90 nm.

The production at any level in the ionosphere is proportional to the product of the gas concentration and the intensity of the radiation. At the top of the atmosphere, the production is small because the gas concentration is small, but as the radiation travels down the gas concentration increases and so does the production rate. Below a certain height, the radiation decreases due to the continual absorption and this creates a level where the rate of production will be a maximum. This level occurs at approximately 150 km.

Recombination is a factor that limits the peak density values. The recombination rate is the rate at which electrons and ions combine to form neutral molecules or atoms. There are generally two main ways in which electrons and ions recombine, they are:



The magnitudes of the recombination coefficients associated with these processes are very different. Due to the conservation of momentum and energy, radiative recombination is less likely since the end products are one particle and one photon. Since the end products for dissociative recombination are two material products, the

conservation laws are more easily adhered to. This rate depends on the type of ions that exists and thier corresponding interaction with the neutral gas. A substantial difference in recombination rates is the fact that when molecular ions are present, they have a much faster recombination rate with electrons through dissociative recombination than atomic ions do (typically by a factor of the order of 10^4). Since atomic ions recombine with electrons at a relatively slow rate, there's actually a better chance for atomic ions to interact with a neutral molecule to form a molecular ion (by charge-exchange or ion-atom rearrangement). After a molecular ion is formed, it can then in turn recombine with electrons by the much quicker dissociative recombination.

The concentration of molecular constituents available for recombination reactions decrease with increasing altitude. The life times of atomic ions become longer and longer at higher altitudes. This causes the regions near and below the F1 region to be dominated by by molecular ions and the overlying F2 region to consist mainly of atomic ions (mostly O^+).

The production and recombination rates discussed here are what Chapman (1931) purposed was responsible for the density peaks observed in the ionosphere. This explains the E and F1 peaks, but not the F2 peak. The F2 peak, at about 300 km, occurs because the production rate of O^+ ions is greater than the recombination rate of atomic ions. This is true up to about 300 km where vertical diffusion is allowed to take place

due to the tenuous nature of the atmosphere at this level. The diffusion allows ions that are formed at higher levels to be pulled down by gravity where they can charge-exchange with molecules. This downward diffusion of ions increases the loss rate of atomic oxygen to a level that's above the production rate of atomic oxygen and the net result is a decreasing ion concentration above 300 km.

Ionization can be produced and destroyed, but the concentration of ionization can also change if it is transported into or out of an area. The earth's magnetic field permeates the ionosphere and is important when considering transportation of a plasma. Individual charged particles are held to helical paths around lines of magnetic induction by the Lorentz force. The characteristic gyro-frequency is denoted by $\omega_{i,e}$. Collisions with neutral particles are very important in the ionosphere. The collision frequency of the ions with neutral particles (ν_{in}) is equal to the gyro-frequency of the ions near 120 km. Below 120 km ions can't move uninterrupted in their gyrating orbits, they will move across the field line in the direction of the wind. Above 120 km ions are tied to the field lines unless an electric field is present. An electric field will cause charged particles to move perpendicular to both the magnetic and electric field according to the $\mathbf{E} \times \mathbf{B}$ drift. Electrons behave similarly except ν_{en} and ω_e are equal near 90 km.

Neutral winds blowing perpendicular to magnetic fields are quite ineffective in transporting ions at F region altitudes

where v_{in}/ω_i is small. The wind component along the magnetic field line tends to move the plasma along the field line. An equatorward wind will push the plasma up the field lines and a poleward wind pushes the plasma down the field lines due to the slope of the magnetic field.

1-2 Electron and Ion Temperatures

The electron and ion temperatures in the F region of the ionosphere are determined by the competition between various heating, cooling, and energy flow processes. The main physical processes that govern the electron and ion temperatures will be discussed in the following paragraphs.

1-2(A) Electron Heating and Cooling

At low and mid-latitudes solar EUV radiation is the primary source of energy in the ionosphere. The energy photoionizes the neutral constituents of the upper atmosphere, producing free electrons and ions. The photoionization occurs predominantly at lower levels of the ionosphere where neutrals are abundant.

The energy carried by the ionizing solar photons exceeds the energy required for ionization of neutral constituents. Conservation of momentum requires that the excess energy goes equally to the electrons and the ions. The energy is divided between the two particles according to the inverse of their masses, so the electrons gain more energy than the ions. Typically, photoionization produces photoelectrons with initial energies of some tens of electron volts. As the photoelectron

travels through the atmospheric gases, it loses excess kinetic energy by excitation of neutral atmospheric gases. At energies of less than 2 eV, the number of excitation processes become small and energy can be passed to other particles by elastic collisions. Due to the massive size of the ions and neutrals compared to the electrons, most of the energy is passed to the ambient electron gas.

When photoelectrons lose their energy at an altitude near where they are produced, the heating is said to be local, while if the photoelectrons lose their energy over a distance greater than a neutral scale height, the heating is called nonlocal. Nonlocal heating effects occur at high altitudes where ambient densities are low and photoelectron energies are high. If photoelectron energies are high enough, they can escape the ionosphere and travel along geomagnetic field lines and deposit their energy in the conjugate ionosphere.

There are a number of different ways in which an electron gas is cooled. Below the F1 layer, where molecular species are plentiful, vibrational and rotational are the main processes that cool the electron gas. Above the F2 peak Coulomb collisions with ions become important and under certain conditions elastic collisions with neutrals cool the electrons.

1-2(B) Ion Heating and Cooling

In the F region ions receive most of their energy from thermal electrons. The ions are preferentially heated over the

neutrals since the heating comes from collisions with charged particles (Coulomb collisions). Thermal electrons provide ions energy as opposed to photoelectrons because the coulomb cross section varies as the inverse of the relative velocity between the colliding particles. The slower thermal electrons have a larger collision cross section with the ions than the faster photoelectrons. The primary source of ion heating is the electron cooling rate (coulomb collisions with the ions).

Another ion heating source is frictional heating by means of neutral winds. Since the ion-neutral collision frequency (ν_{in}) is greater than the electron-neutral collision frequency (ν_{en}), the ion gas is heated.

Ions cool by transferring energy to the neutrals. The rate of cooling depends on the temperature difference between the two gases and also the possible difference in their bulk velocities (frictional heating).

At high temperatures the interaction between an ion and its parent neutral is dominated by resonant charge transfer. This process has the effect of replacing a hot ion with a cold one and is an important mechanism for removing energy from an ion gas.

1-2(C) Electron and Ion Thermal Conductivity

Energy in the ionosphere can be added, taken away, and also be transported by conduction. The change in temperature would be determined by the divergence of the heat flux. In a fully ionized gas, the thermal conductivity is primarily due to

electron-electron and electron-ion interactions. When a magnetic field is present, the motion of the electrons is modified and the conductivity becomes anisotropic. The heat flow will be parallel to the magnetic field lines and in any other direction the conductivity is reduced by $\sin^2 I$ (I =magnetic dip angle). This is due to the fact that the charged particles spiral along the magnetic field and don't move across the magnetic field due to the Lorentz force. In the ionosphere above 300 km, the fully ionized approach can be used. Below 300 km, the ionospheric plasma becomes weakly ionized. The effect of electron-neutral collisions on the conductivity must be included. The thermal conductivity decreases by the addition of electron-neutral collisions. This effects the ionosphere during the day at altitudes below 150 km because electron density at 200 km increases and this offsets the effect of the neutrals. At night, when electron density decreases, the decrease in thermal conductivity reduces thermal conduction below 200 km. The electron temperature is only dependent on local energy production and loss. This essentially decouples the high altitude electron gas from the E and sometimes F1 regions of the ionosphere. The regions of the ionosphere below the F2 peak are essentially unaffected by the magnetospheric heat fluxes into or out of the ionosphere.

The ion heat flux is defined the same as the electron heat flux. Here, ion-neutral collisions will decrease the ion thermal conductivity just as electron-neutral collisions decreased the

electron thermal conductivity. These neutrals only affect the ion conductivity below 300 km. Because of the much larger mass of the ions, the ion conductivity is much smaller compared to the electron (due to much slower thermal velocities). The larger mass also increases the size of the Larmor radius (r_L) and decreases ion gyro-frequency. This results in fewer gyrations around a magnetic field line before there is a collision. The conductivity perpendicular to the magnetic field is due to the ions and that parallel to the field is caused by the electrons.

1-3 Neutral Winds at Ionospheric Heights.

Neutral wind circulation at ionospheric heights is important because even at the F2 peak where ionization is at its densest value, only about 1% of the total atmosphere is ionized. The neutral atmosphere's motions will be of major importance in understanding the changing ionospheric parameters because of neutral-charged particle collisions.

Neutral motions in the thermosphere were first calculated by Jacchia (1965) when observing orbital changes in satellites due to drag effects. The neutral atmosphere with density ρ slows down the velocity of the satellite. As the atmosphere is heated, it expands and the atmospheric density at the satellite's altitude will increase. The amount of satellite drag gives an indication to the density and thus the temperature of the neutral atmosphere. During the day, thermal expansion of the atmosphere forms what is known as

the diurnal bulge. It is centered on the equator at about 1400 LT (see figure 1-2). The bulge creates horizontal pressure gradients which cause horizontal winds. Winds at thermospheric heights are influenced by the coriolis force and even more strongly by viscosity and collisions between ions and neutral particles (ion-drag force). The ion-drag force is the limiting factor in the wind speed at these altitudes (above 200 km). The winds blow away from the hottest sections of the atmosphere to the coldest. Because of the ion-drag force, the winds blow poleward during the day and equatorward at night. This is quite different from the lower atmosphere where winds are more strongly controlled by the coriolis force, which causes circulation around low and high pressure areas.

Neutral winds cause movements of ionization along magnetic field lines. The ionization will raise and lower according to the wind direction. An important consequence of this changing of altitude is seen when the height dependency of recombination rates is taken into account. Several interesting effects in the F2 region (diurnal variation of h_{max} and peak electron concentration) can be described in terms of the winds.

During a geomagnetic storm, large heat inputs are put into high latitude regions. These heat inputs can exceed the quiet time solar inputs (because the heat is concentrated in small areas of the auroral oval) and a storm time circulation can be superimposed on the quiet circulation (see figure 1-3).

Depending on the time of the high latitude heating, the storm circulation can either enhance the quiet time flow or oppose and even override the quiet time flow.

Figure Captions for Chapter One

Figure 1-1 A typical electron density height profile of the ionosphere over Arecibo.

Figure 1-2 Neutral temperature distribution at 300 km based on an empirical model. The arrows represent wind speeds. The longest arrow corresponds to a wind speed of 225 m/s (from Dickinson and Geisler, 1969; and Roble, 1977)

Figure 1-3 (a) Schematic view of high-latitude heating processes that affect neutral air motions. (from Banks and Evans 1979); (b) Sketch of the circulation set up by large heat inputs from geomagnetic storms. (from Rishbeth, 1975)

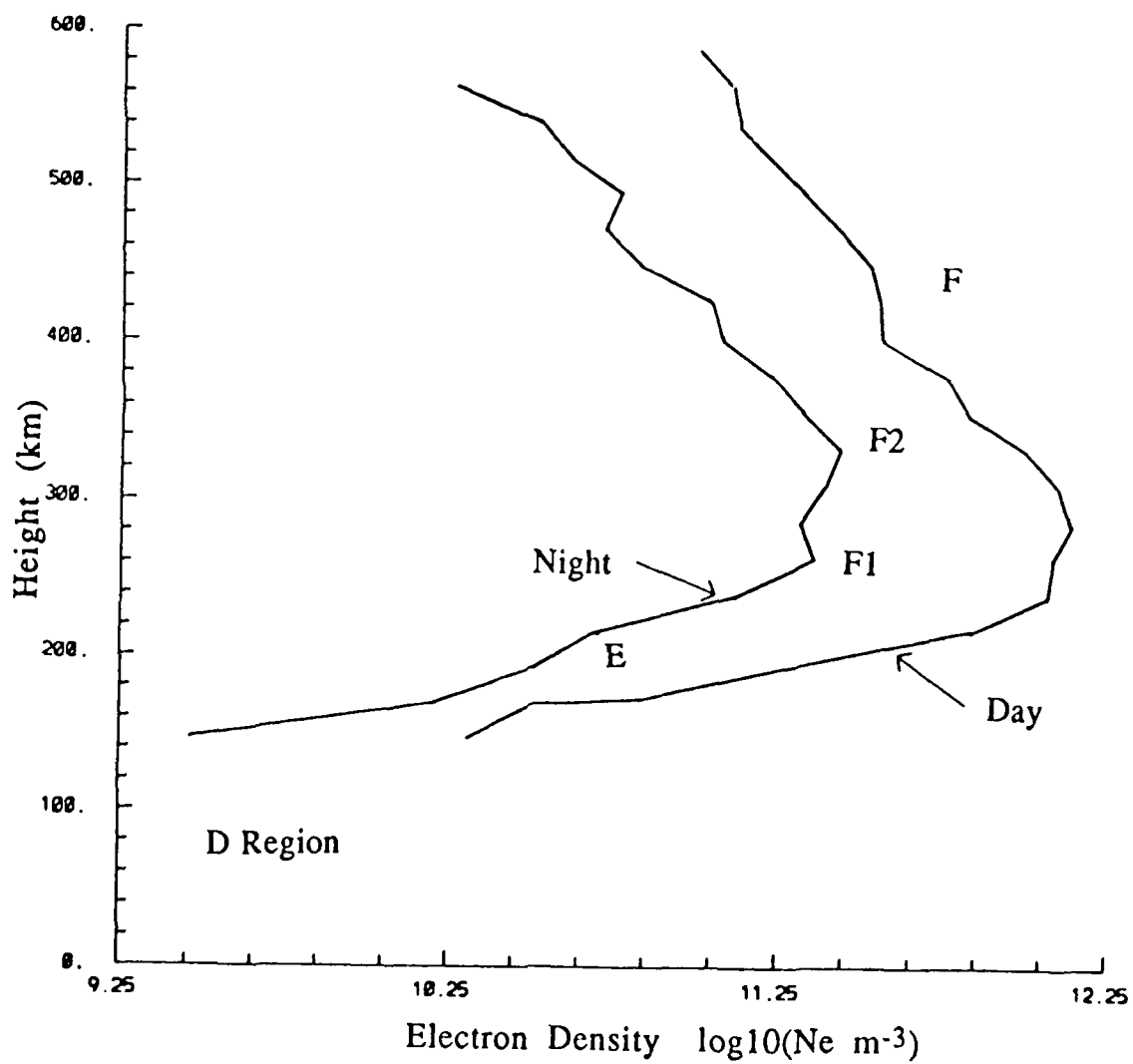


Figure 1-1

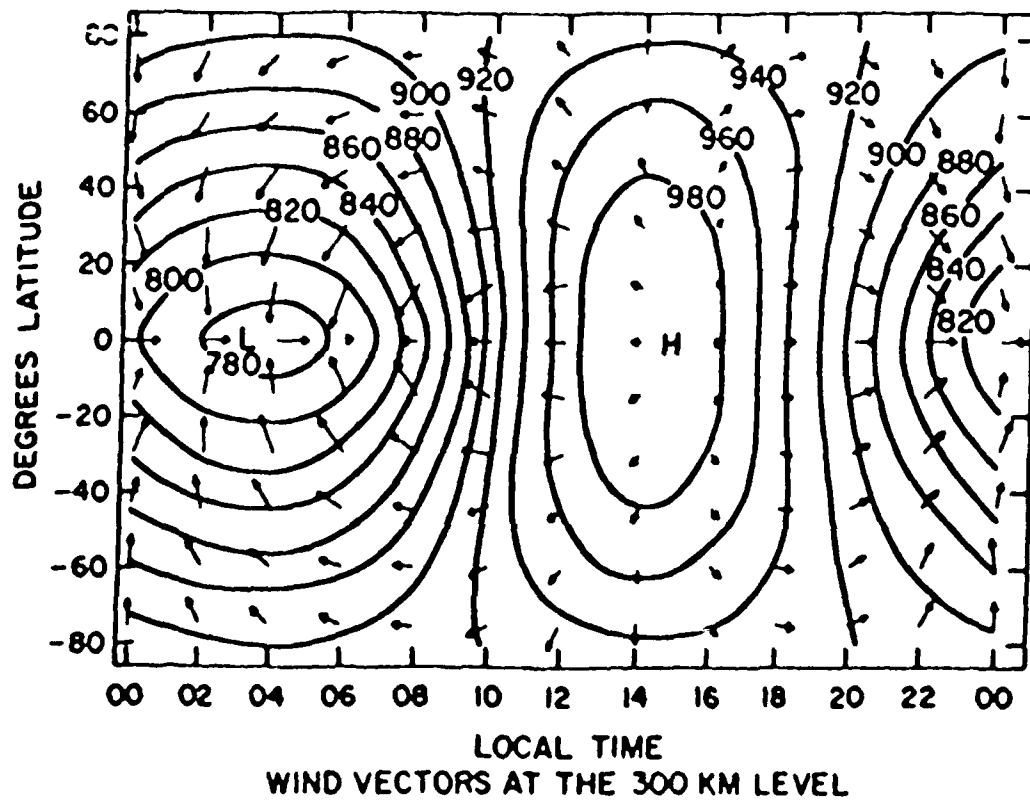


Figure 1-2

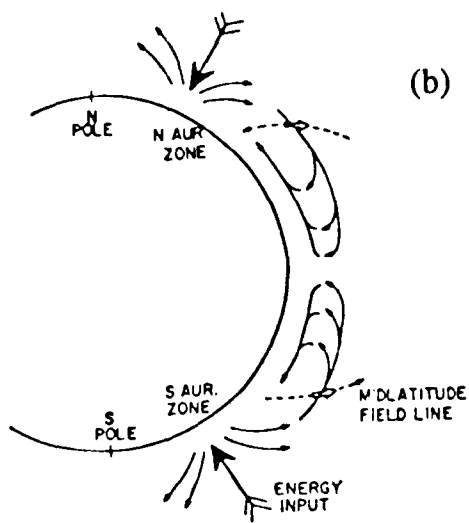
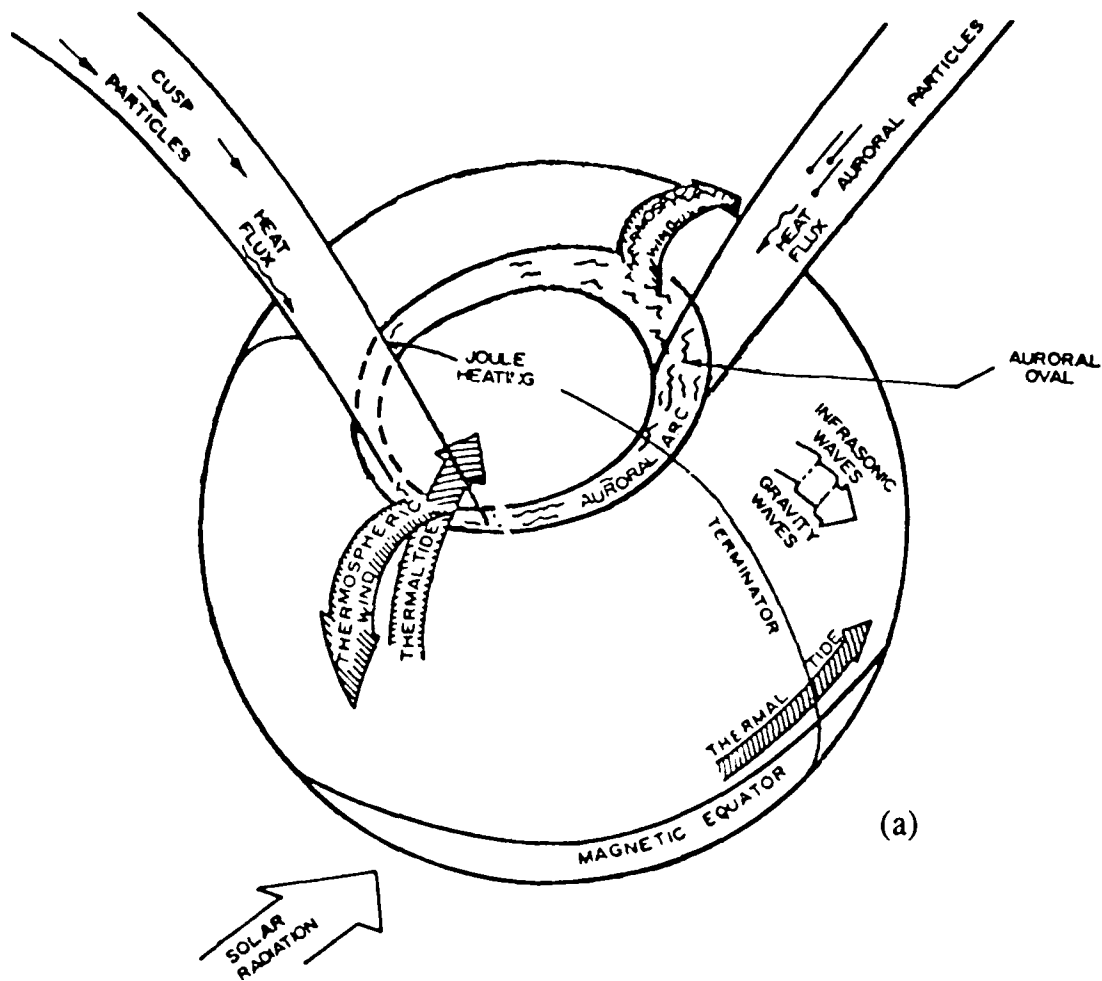


Figure 1-3

Chapter 2 The Incoherent Scatter Radar

The incoherent scatter radar works on the principle that electrons can scatter electromagnetic energy. It's not the intent of this chapter to fully describe the incoherent scatter technique. A brief explanation of the theory and determination of the ionospheric parameters used in this study will follow.

2-1 Theory

2-1(A) Scattering of Radiation by Free Electrons

When an electromagnetic wave is incident on an ionized gas, the electric field of the incoming wave causes the electrons to oscillate. The moving electrons will in turn radiate due to their acceleration. The electrons oscillate at the incident wave's frequency plus or minus an amount due to the Doppler shift caused by the thermal motions of the electrons. Since the electrons are in random thermal motion, and energy scattered by each electron will be in different phases, the sum of the scattered radiation in any direction except the incident beam's direction will be incoherent. Thus the term Incoherent scatter comes from this principle.

The fraction of the incident energy flux that is re-radiated (also known as the scattering cross section) is $8\pi(r_e)^2/3$; where r_e is the classical electron radius ($= e^2/\epsilon_0 m_e c^2$) and $e^2 = (q_e)^2/4\pi\epsilon_0$. The amount of energy scattered by an electron into a unit solid angle per unit incident flux is given by

$(r_e \sin \psi)^2$. The angle ψ is the polarization angle, which is the angle between the incident electric field and the observer. Using the idea of cross section above, the radar cross section of an electron is $\sigma_e = 4\pi(r_e \sin \psi)^2$ and the power of the signal received at the radar receiver would be due to the density of the electrons (radar cross section $(\sigma) = N\sigma_e$, where N = number density of the electrons).

2-1(B) Scattering of Radiation by Density Irregularities in an Ionized Gas

Scattering of radio waves originates from individual electrons, but stronger scattering occurs from density irregularities in the ionosphere. These irregularities occur due to the random thermal motions of the ions and electrons. The electrons and ions can't move independently of one another due to electrostatic forces. Any irregularities will be kept from existing that way due to the electrostatic repulsion from like charges. This will cause fluctuations in electron and ion densities. In view of the much greater mass of the ions, the rate of ion fluctuations is slower than that of the much lighter electrons. The electrostatic field is composed of a fast and slow fluctuating components. The fast fluctuating part almost completely cancels the electron density fluctuations, but has a negligible effect on the ions. The slow fluctuating part of the field affects both the motion of the electrons and ions. Even though the electrons are under the influence of the slow

fluctuating component of the electrostatic field, they still have time to assume an equilibrium distribution due to their low inertia. The instantaneous electron distribution is almost identical to the instantaneous ion distribution. This coupling of the electrons distribution to the ions decreases the Doppler broadening of the scattered signal. An equivalent result is achieved if it is assumed that the radar cross section is reduced by two. ($\sigma = 1/2N\sigma_e$).

To see the connection between the electronic and ionic motion, the Debye length (λ_D) must be considered. The Debye length indicates the distance over which the charge on a single electron is effectively connected to an ion in a plasma. This is the distance in which an electron's motion can be thought as being cooperative with the ions.

If the investigating radio wavelength (λ) is less than the Debye length (λ_D), the radar cross section (σ) = $N\sigma_e$. This indicates that the signal received at the receiver will be Doppler broadened according to the electron velocity distribution. Thus, from the width of the spectrum, the electron temperature can be deduced and the magnitude of the power received is directly proportional to the number density of the electrons. However, the radar frequencies currently used (40 - 1200 MHz) have wavelengths which are much larger than the Debye lengths in the ionosphere (one - several cm).

When $\lambda > \lambda_D$, the $\sigma = 1/2N\sigma_e$. The scattered energy will have contributions from both the electrons and ions. The width

of the power spectrum is much narrower due to the slower ion component being included. The actual return is from the electrons, but the electrons are controlled by the thermal speed of the ions. This narrowing of the bandwidth makes the signal much easier to detect. The shape of the spectrum changes from a gaussian shape (when $\lambda < \lambda_D$) to a double-humped shape resulting from both the electron and the ion components of thermal velocity being included. There is a parameter α which describes the scattering by the ratio of electron debye length to radar wave length ($\alpha = \lambda_D/\lambda$).

If $\alpha \gg 1$ ($\lambda < \lambda_D$), the scatter will be from the electrons. The Doppler broadening will cause the retrieved power to be gaussian-shaped (assuming a maxwellian velocity distribution for electrons in the ionosphere).

If $0.5 < \alpha < 2.0$, the scattered energy will have approximately equal contributions from both the electrons and the ions. (This is the double-humped case).

If $\alpha \ll 1$ ($\lambda > \lambda_D$), the effect of the electrons is decreased and the power appears as a single line, Doppler shifted approximately equal to the plasma frequency (f_n).

$$f_n = \frac{1}{2} \left(\frac{N_e e^2}{m_e \epsilon_0} \right)^{1/2}$$

The largest part now corresponding to the ion component. The parameter α reflects the amplitude and shape of the power frequency spectrum.

2-1(C) Unequal Electron and Ion Temperatures

In the ionosphere the electrons and ions are not in thermal equilibrium. This causes the double-humped shape of the power spectrum. The electron temperature (T_e) varies much more than the ion temperature (T_i) and this affects the shape of the spectrum. As T_e increases, the space charge distances increase, and this increases the electrostatic field. This increase in the electric field will cause smaller ion fluctuations and thus decrease the amplitude of the power spectrum. The end result is the width of the power spectrum can be determined by the ion temperature and the ratio T_e/T_i controls the height of the two maxima relative to the "valley" between them.

2-2 Determination of Physical Parameters

2-2(A) Electron Density.

Electron density in the ionosphere can be determined in several different ways by using the incoherent scatter radar. The most common is the power profile method.

Power Profile Method.

Using the ranging technique of a pulsed signal and measuring echo power (P_s) seems like a good way to obtain electron density as a function of height, $N(h)$.

$$P_s = \text{Const.} \frac{N(h)\sigma(h)}{h^2}$$

The constant in this equation can be calculated by careful determination of radar parameters (power transmitted, area of

receiving antenna, pulse length, and others) or by calculating the electron density by some other means (using a nearby ionosonde and measuring the penetrating frequency of F2 layer).

From theory, we know that the cross section, $\sigma(h)$, depends on the parameter α and T_e/T_i , both which are functions of height. In the ionosphere λ is usually greater than λ_D which makes α go to zero and then we're just left with T_e/T_i . It will be necessary to obtain T_e/T_i from separate spectrum measurements (explained in the next section). Then it is known how the radar cross section (σ) varies with height and $N(h)$ can be calculated directly from echo power.

If α is unknown or doesn't go to zero, then a method described by Moorcroft (1964) can be used. Moorcroft examined the analytical expression for the spectrum of an ionized gas and showed that the spectral shape is the same for $\alpha < 1$ as it is for $\alpha \ll 1$ but with a temperature ratio $(T_e/T_i)/(1+\alpha^2)$. This says that the shape of the spectrum depends on α in the same way it depends on T_e/T_i .

Let's say α goes to zero, and then T_e/T_i changed to counteract the change in α , then the shape would remain the same.

$$T_e/T_i = (1+\alpha^2)\beta, \quad (\text{where } \alpha \leq 1)$$

T_e/T_i is the true value of electron to ion temperature ratio and β is the fictitious change in T_e/T_i to keep the shape of the

spectrum constant for a change in α (as it goes to zero) or becomes very small.

$$\sigma = \sigma_e / (1 + \beta) \quad (\text{where } \sigma_e = 4\pi r_e^2)$$

To use this, let $\alpha = 0$ and calculate what the shape of the spectrum would look like. Then look at observed shape of the spectrum, the difference leads to the determination of β . The scattering cross section at that level can be determined and then electron density can be calculated. This method is somewhat indirect, but gives good results.

2-2(B) Electron and Ion Temperatures

Recall that the width of the scattered signal spectrum is controlled by the ion temperature and both T_e/T_i and α control the shape of the spectrum. In the case where α is small, T_e/T_i controls the shape of the spectrum (Fig. 2-1). By careful measurement of the shape of the spectrum the temperatures may be deduced.

When α can not be assumed to be small, or if it is unknown, then a method (already described) by Moorcroft (1964) can be used. This leads to $T_e/T_i = (1 + \alpha^2)\beta$, where $\beta = T_e/T_i$ deduced for $\alpha \leq 1$ (see the previous section).

This can be used in σ approximately equal to $\sigma_e / (1 + \beta)$ to get an estimate of electron density through the cross section (σ). This approximation leads to a reasonably close density profile from scattered power received at the ground antenna. By measuring the width of the spectrum at the half-peak-

power point, it is possible to obtain ion temperature (T_i). If T_i , N , and β are known, the electron temperature (T_e) can be solved for.

2-2(C) Spectrum Changes Due to Particle Motions

So far, the plasma as a whole has been assumed to be stationary. Motions in the plasma of the ionosphere can also be detected by back-scattered radiation. We must first look and see what effect plasma motion will have on the scattered energy spectrum.

The simplest case for plasma motions is when both the electrons and ions drift as a whole toward or away from the radar. If the speed of the drift is V_d , then the entire spectrum will be shifted by an amount Δf_d (where $\Delta f_d = 2V_d/\lambda$). The shape of the spectrum won't be changed, just shifted due to the motion of the plasma.

Electrons and ions don't always move together. If the ions were stationary relative to the radar and the electrons were moving, then an asymmetry would result in the double-humped curve with no shift in frequency (shape change only). With both electrons and ions moving, the spectrum would change in both ways (fig. 2-2).

2-2(D) Electric Field Determination.

Perpendicular drift velocities in the ionosphere are connected with the magnitude and direction of electric fields. An electric field in the F-region of the ionosphere will cause the

plasma to drift across the magnetic field lines due to a force known as the $\mathbf{E} \times \mathbf{B}$ force. This force is perpendicular to both the \mathbf{E} and \mathbf{B} fields.

$$\mathbf{V}_{\perp} = \frac{\mathbf{E} \times \mathbf{B}}{B^2}$$

The electric field can be deduced by pointing the radar beam perpendicular to the magnetic field and measuring movements of the ions. Electric field drifts can set the neutral air into motion and this affects the velocity component of the ions parallel to the magnetic field, so both parallel and perpendicular components should be measured at the same time.

All of the the radar parameters have not been described here, only those which that are used in the upcoming study. The significance of the incoherent scatter radar is its capability of measuring many different parameters throughout virtually the entire extent of the ionosphere simultaneously.

Figure Captions for Chapter Two

Figure 2-1 Dependence of the power spectrum on the T_e/T_i ratio. (from J.V. Evans, 1974)

Figure 2-2 Power spectrum reaction to various drift conditions (a) no drift, (b) ion drift at one tenth the mean ion thermal velocity, (c) electron drift at 0, 0.1, and 0.2 times the mean electron thermal speed, (from J.V. Evans, 1974)

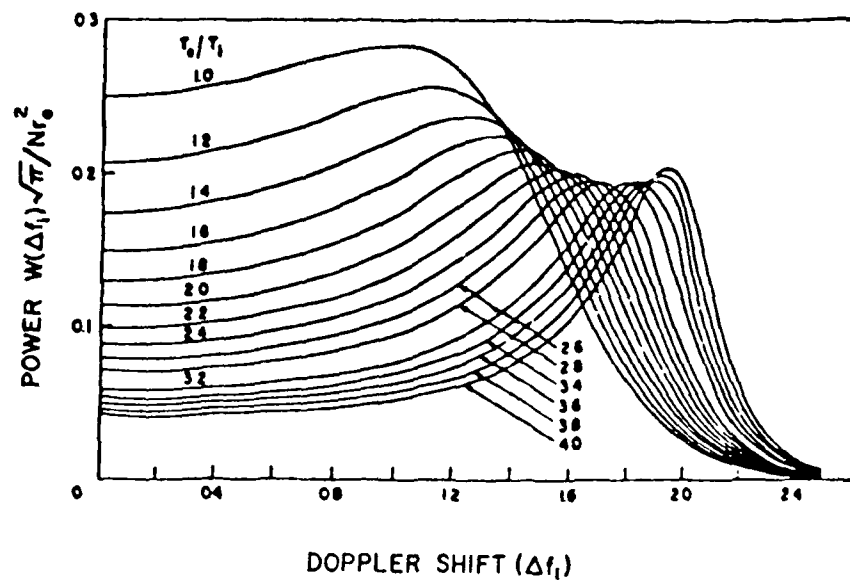


Figure 2-1

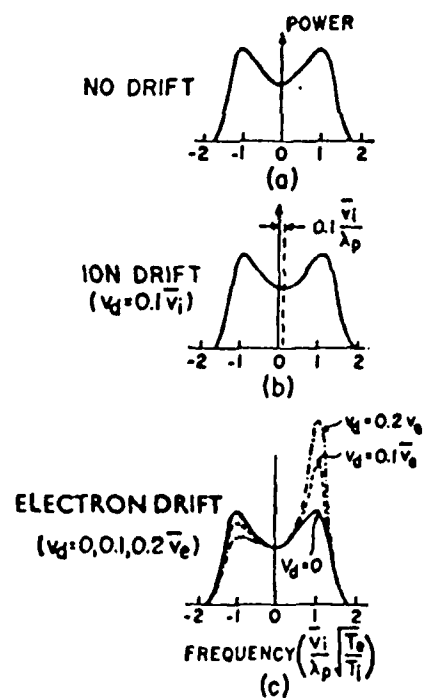


Figure 2-2

Chapter 3 The Quiet Ionosphere

The Millstone Hill incoherent scatter radar investigates the topside ionosphere from 235-600 km. The 18th of September 1984 is a geomagnetically quiet day (see figure 4-1). A description of the quiet ionosphere from radar observations of electron density, electron and ion temperature, and ion velocities follows:

3-1 Millstone Hill Electron Density

The electron density (N_e) pattern in figure 3-1 exhibits a strong diurnal variation. The density starts to increase at 0500 LT and continues to increase until approximately 1700 LT. The decrease in density at sunset is at a faster rate than the increase at sunrise.

The height of maximum electron density (h_{max}) is highest near midnight (300 km) and decreases as dawn approaches. After sunrise the level of h_{max} increases slowly until about midnight when the cycle repeats itself.

The ionosphere expands and contracts according to the sun's diurnal heating cycle. When comparing the density variation with time, it's necessary to remember that the layer is rising and falling throughout the day.

In the morning at all altitudes, the electron density increases till about noon (1100 LT). After the mid-day peak, the density decreases if the fact that the layer rises is taken

into account (compare the density at a fixed height with respect to h_{max}). The density decreases until there's another maximum at 1700 LT. It was suggested by Evans (1965) that this second maximum is caused by the electron temperature falling rapidly due to sunset (see figure 3-2A). This rapid decrease in electron temperature gives rise to a collapse in the layer thickness and an increase in the density at the peak.

3-2 Millstone Hill Electron and Ion Temperatures

The electron temperature (T_e) rises rapidly at sunrise and then remains more or less constant throughout the day. The rate of decrease in T_e at sunset is somewhat less than the increase at sunrise. The rate of decrease in T_e is more gradual because in the late afternoon there's a maximum flow from the magnetosphere (Roble 1975) and electron density decreases. Both of these mechanisms act to slow down the cooling rate of T_e at sunset. The maximum T_e occurs at approximately 1300 LT and the minimum is observed at 0200 LT.

The diurnal ion temperature (T_i) variation tends to follow the electron temperature. This thermal coupling between the ion and electron temperatures is generally seen at 300 km (figure 3-3). The size of the changes in ion temperature is much smaller than that of the electrons due to the ion's greater mass and the radiative transfer process between them.

Between the hours of midnight and 0500 LT, the ion temperature appears to be greater than the electron

temperature (see figure 3-3). It has been shown by Mazaudier and Bauer (1976) that ion temperatures can exceed electron temperatures by up to 50° K in the nocturnal F region ionosphere at Saint Santin. At first one might think this is due to systematic and/or statistical errors which are inherent in the radar measurements, but neither one has been able to be consistent or large enough to account for the temperature difference. To a first order, the three gases (electron, ion, and neutral) are in thermal equilibrium in the nocturnal mid-latitude F region. Since a change in the neutral temperature affects the ion's temperature which in turn affects the electron's temperature (see figure 3-4), the downward increase in the neutral temperature gradient gives the other two gases similar gradients. The heat conductivity for the electron gas is much higher than the ion or neutral conductivity. This results in a downward heat flux for the electron gas. The first order equilibrium that was mentioned is maintained by a heat input to the electrons by the slightly warmer ions.

3-3 Arecibo Electron Density

The radar at Arecibo has measurements of ionospheric parameters from 60 - 565 km. Data is shown for the topside ionosphere (\cong 200 - 600 km) for quiet geomagnetic conditions.

The quiet time ionosphere over Arecibo will be represented by measurements taken on 17 October 1984. This is due to a data gap from a radar failure on 18 September

1984. The data from 17 October 1984 is still in the equinox transition period.

The electron density in figure 3-5 also exhibits a strong diurnal variation. At 0600 LT density increases until about 1430 LT when it reaches a maximum. Besides there being only one maximum, Arecibo's density pattern parallels the Millstone Hill pattern until midnight.

At midnight the height of h_{max} is near its highest level (350 km). Instead of gradually decreasing until dawn, as at Millstone Hill (see fig 3-1), h_{max} starts a 100 km drop just after midnight. This happens at a time when the parallel direction of the ions indicate a downward motion (fig 3-6A) and there is no indication of strong electric fields from perpendicular ion drift measurements (figure 3-6B). This indicates that the drop in h_{max} is due to a poleward wind just after midnight. Then, at 0400 LT the height of h_{max} rises sharply to about 300 km. This rise occurs when the poleward wind starts to subside (see 3-6A). The density at low altitudes is decreased by higher recombination rates and h_{max} returns to higher altitudes. The height of h_{max} then continues to decrease as sunrise approaches. There is then a slow increase till 1500 LT when another drop occurs lasting about three hours and then h_{max} increases after sunset to its maximum value at midnight.

This difference in the behavior of h_{max} after midnight compared to Millstone Hill is known as the "post-midnight collapse". This is different than electron density patterns

observed at higher or lower latitudes. This could be due to the fact that Arecibo is located at a low latitude geographically speaking, but at a middle geomagnetic latitude (30° N). A semi-diurnal component in the neutral winds has been associated with the h_{\max} decrease just after midnight by Behnke and Harper (1973) and Harper (1973). When the normal quiet-time equatorward wind stops or even turns poleward, the ionization starts to slide down the field lines. Since diffusion velocity in the downward direction decreases with decreasing altitude, an increased concentration in plasma density results in the bottomside ionosphere. This increased electron density lasts until the higher recombination rates in the bottomside ionosphere along with the commencement of the eastward electric field at 0400 LT decrease electron density to lower values.

3-4 Arecibo Electron and Ion Temperatures

The electron temperature (figures 3-7 and 3-8) at Arecibo rises rapidly at sunrise. It increases until around 1030 LT and then decreases in the afternoon. The decrease in electron temperature is associated with an increase in electron density. When electron density increases, the electron cooling rate also increases due to the increased number of ions. The electron temperature continues to decrease until 1500 LT and then increases till 1700 LT. Several things change at 1500 LT: The semi-diurnal component of the wind causes a downward

motion in the direction of the ionization along the field lines (figure 3-6A) which brings plasma of increased temperature to lower altitudes. The downward motion of plasma pushes the electrons into a region of increased recombination rates. This along with a decreasing solar zenith angle decreases the electron density and the cooling rate of the ions. Energy is supplied to the electrons from the sun until it sunset occurs after 1700 LT. Electron temperature then decreases through the early morning hours until sunrise and this completes the cycle.

The ion temperature doesn't change as drastically as the electron temperature (see figure 3-8), but does show the diurnal variation. At 1000 LT the ion temperature increases and stays more or less constant until 1800 LT after sunset. The diurnal variation is the only noticeable change in ion temperature.

3-5 Parallel Ion Velocities

The ion velocities, actually anti-parallel ion velocities, are plotted for Millstone Hill, Arecibo, and Saint Santin incoherent radar sites. Since anti-parallel ion velocities are plotted, positive velocities indicate motion up the magnetic field line and negative velocities indicate downward motion along the field line. Poleward meridional winds and/or westward electric fields lead to downward ion motion while equatorward

winds or westward electric fields result in ion motion up along the field lines.

The three plots in figure (3-9) are observations during geomagnetically quiet days. In general there is upward motion along the field lines at night and downward motion during the day. This is especially evident at Millstone Hill and Saint Santin (the locations which are located higher in latitude). This situation agrees well with the quiet thermospheric wind circulation pattern where there are poleward winds during the day and equatorward winds at night. At Arecibo, a semi-diurnal wind effect is seen. This wind effect comes from the fact that the solar heat input is not sinusoidal in nature and harmonics of the order of 24 hours (12, 8, 4, etc...) are seen in the wind pattern.

Figure Captions for Chapter Three

Figure 3-1 Diurnal variation of electron density over Millstone Hill on 18 September 1984. The height of maximum electron density is sketched as a dashed line.

Figure 3-2 Contours of diurnal variation of charged particle temperature over Millstone Hill on 18 September 1984. (a) electron temperature (T_e), (b) ion temperature (T_i)

Figure 3-3 Diurnal variation of electron and ion temperature at 300 km

Figure 3-4 Energy budget of the nocturnal ionosphere including neutrals. (from Mazaudier and Bauer, 1976)

Figure 3-5 Same as figure 3-1 for Arecibo on 17 October 1984.

Figure 3-6 Diurnal variation of ion drifts and height of the F layer over Arecibo on 17 October 1984. (a) antiparallel ion velocity ($-V_{||}$), (b) perpendicular ion velocity in the northward direction ($V_{\perp N}$), (c) height of maximum electron density (h_{max}).

Figure 3-7 Same as figure 3-2 for Arecibo on 17 October 1984.

Figure 3-8 Same as figure 3-3 for Arecibo on 17 October 1984.

Figure 3-9 Antiparallel ion velocities over Millstone Hill, Saint Santin, and Arecibo for geomagnetically quiet conditions.

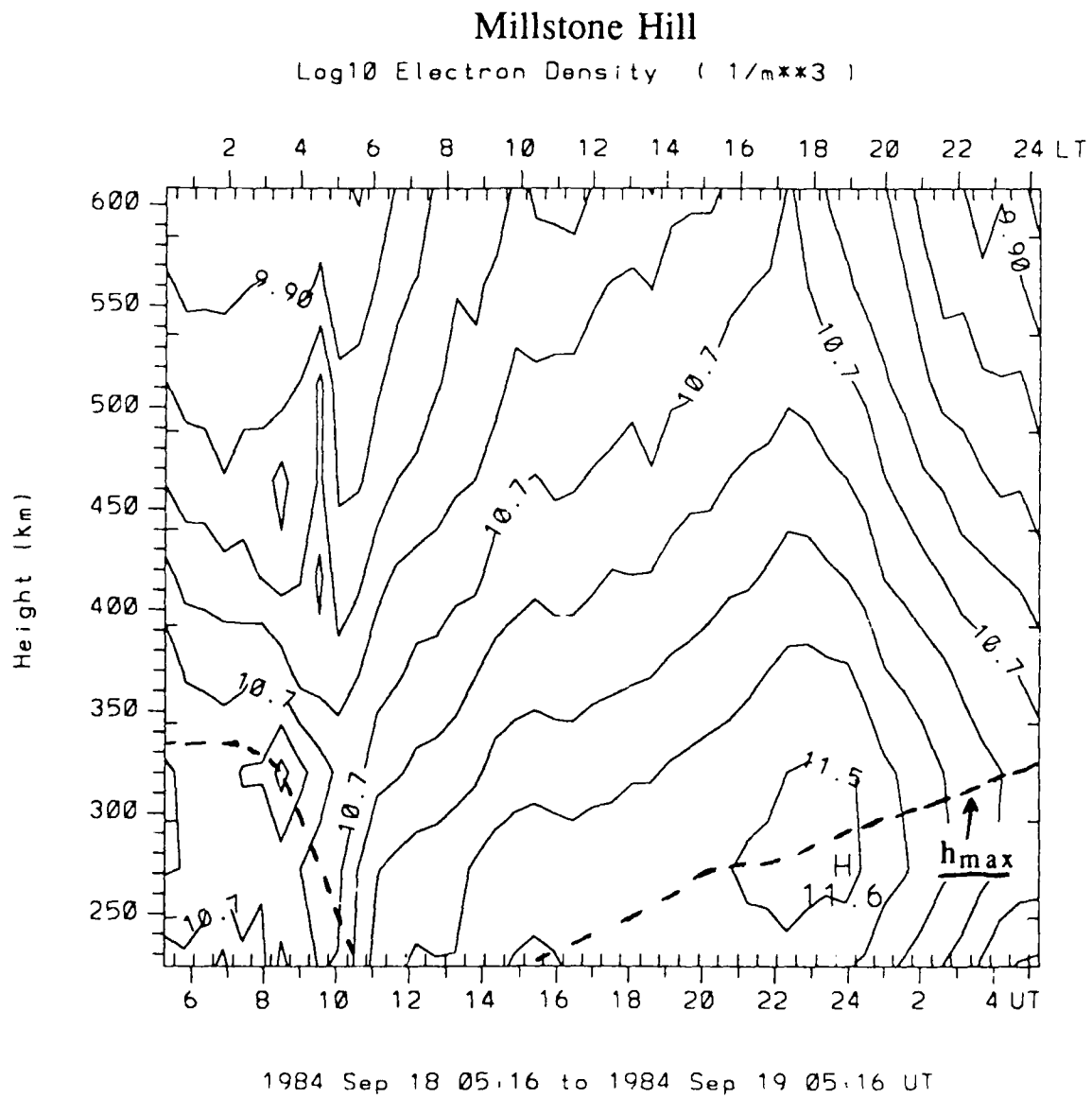


Figure 3-1

UT = LT - 5

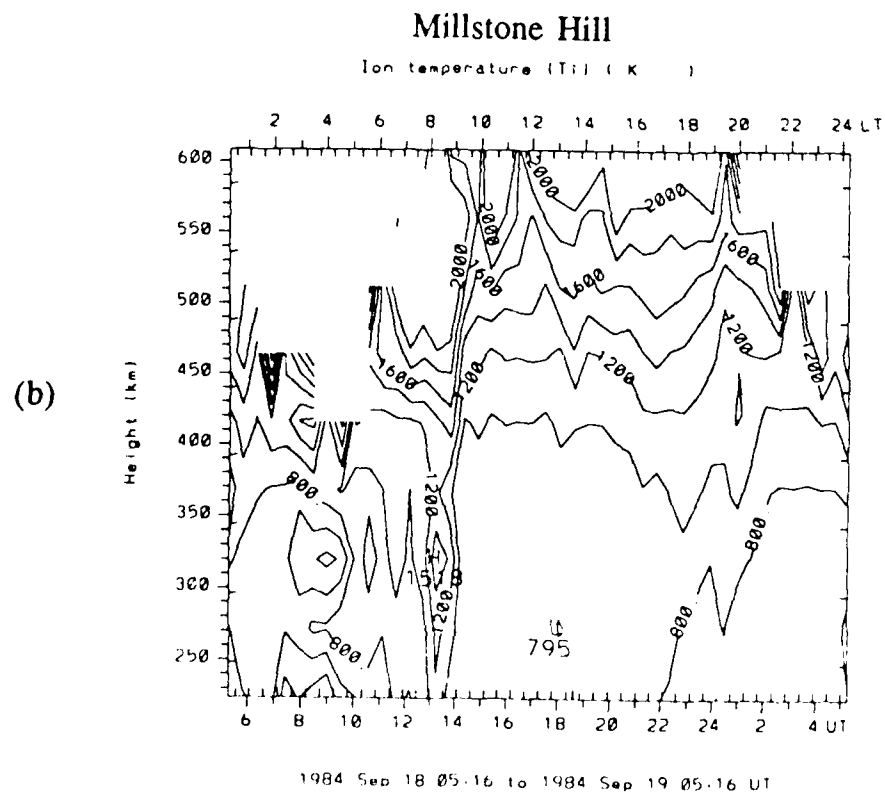
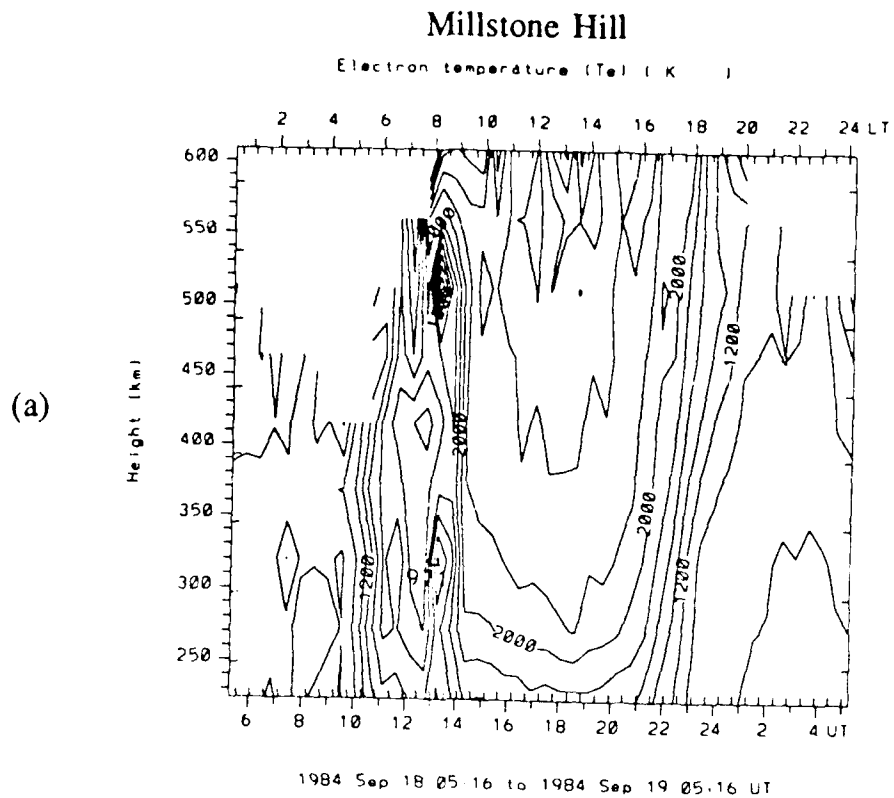
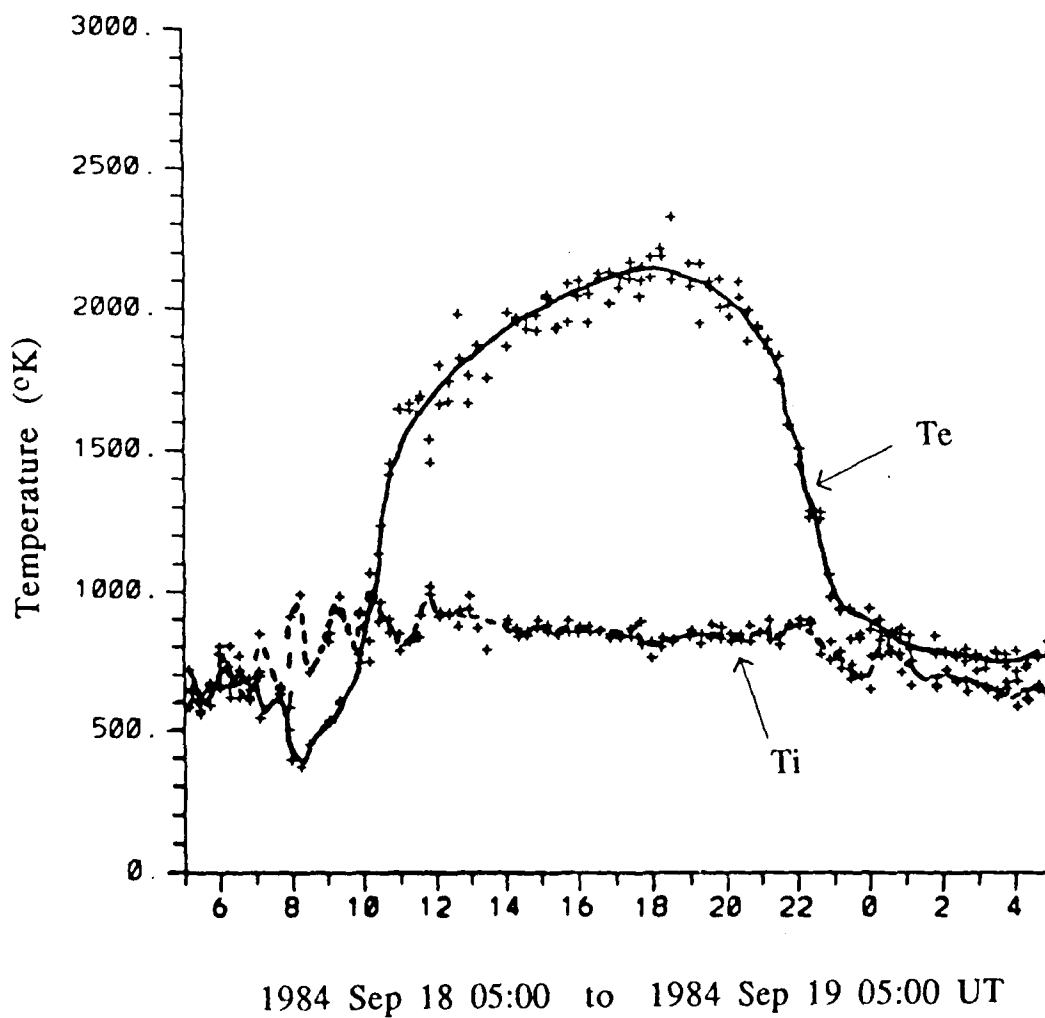


Figure 3-2

Millstone Hill Electron and Ion Temperature - 300 km



UT = LT - 5

Figure 3-3

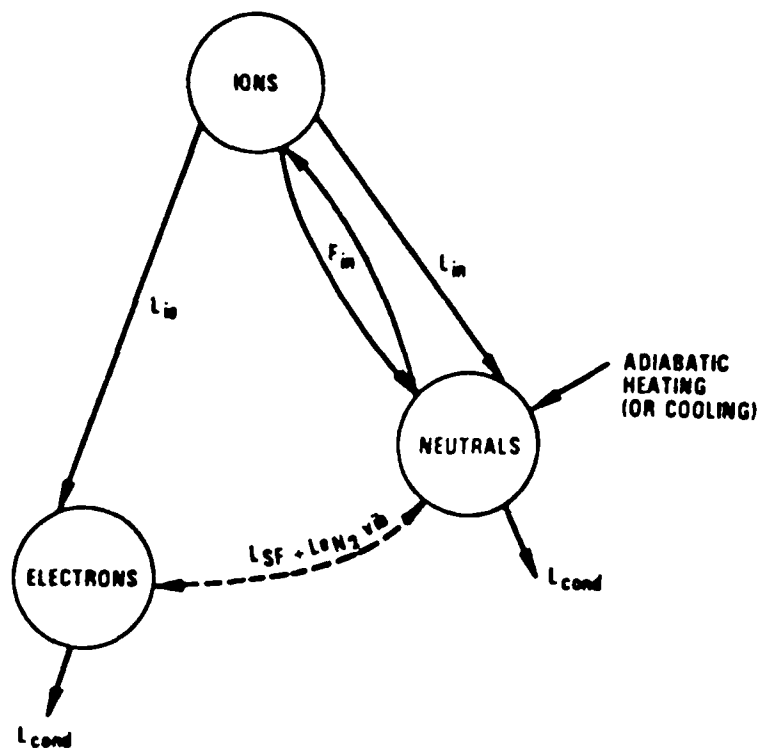


Figure 3-4

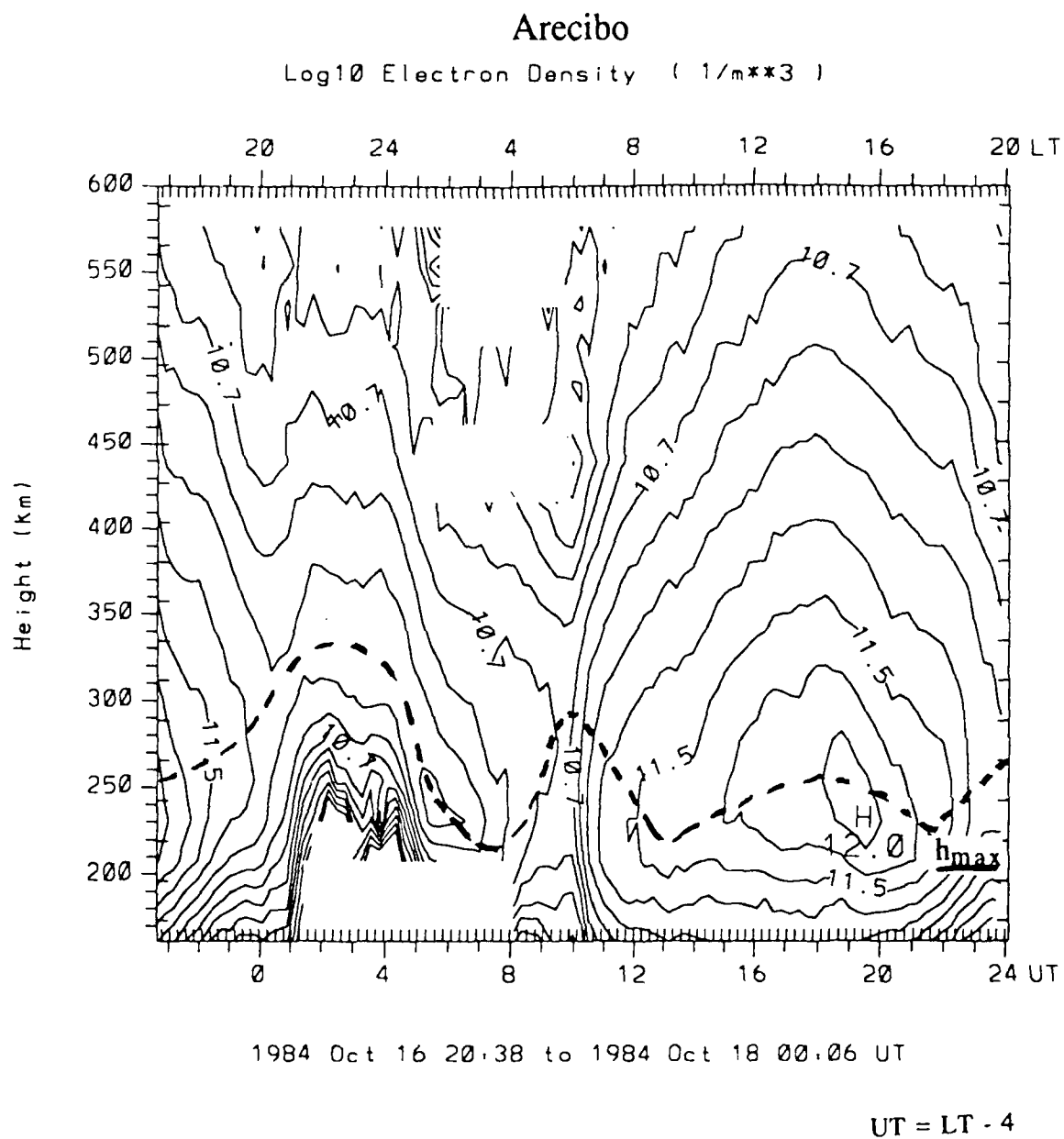


Figure 3-5

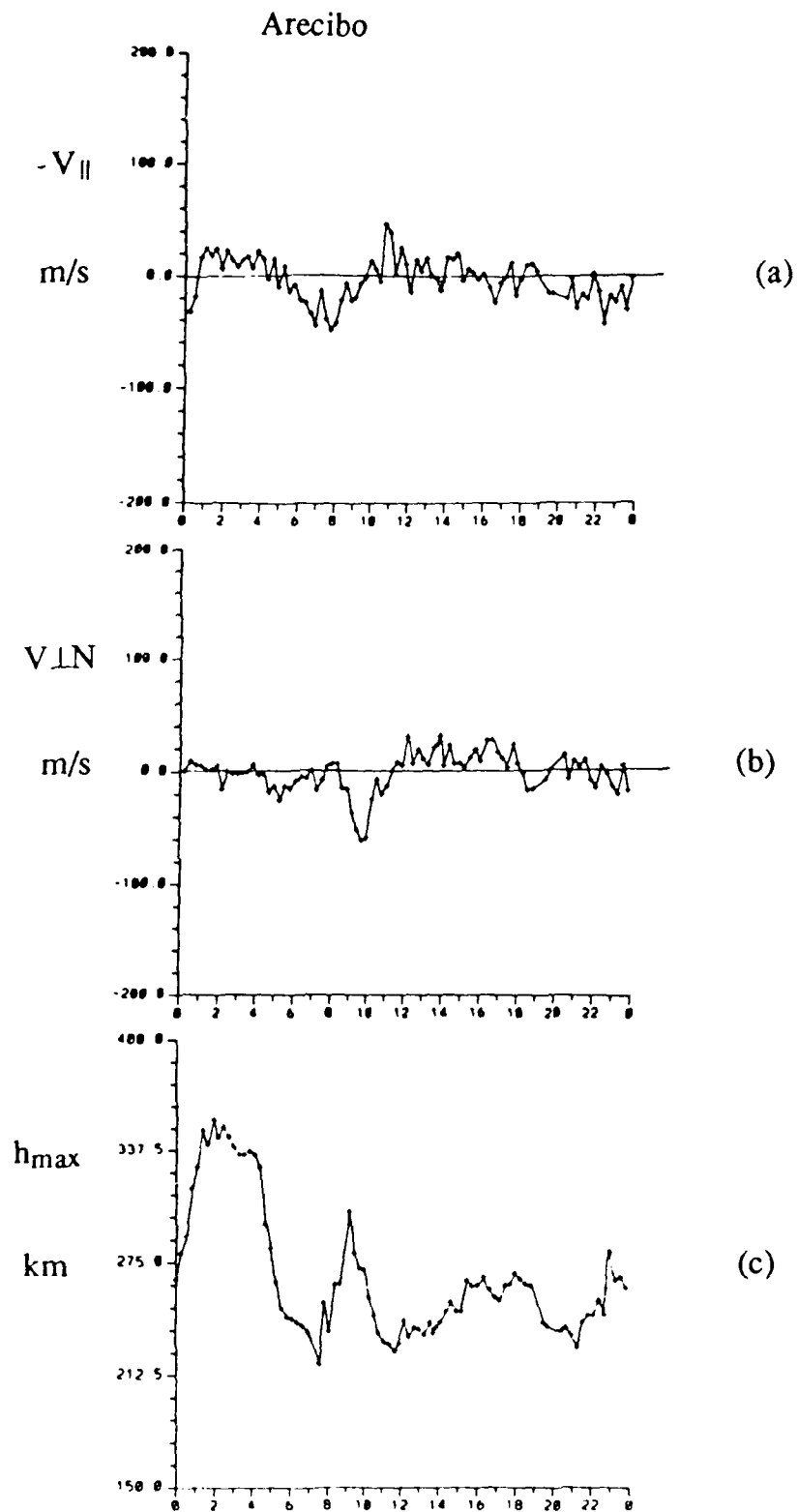


Figure 3-6

UT

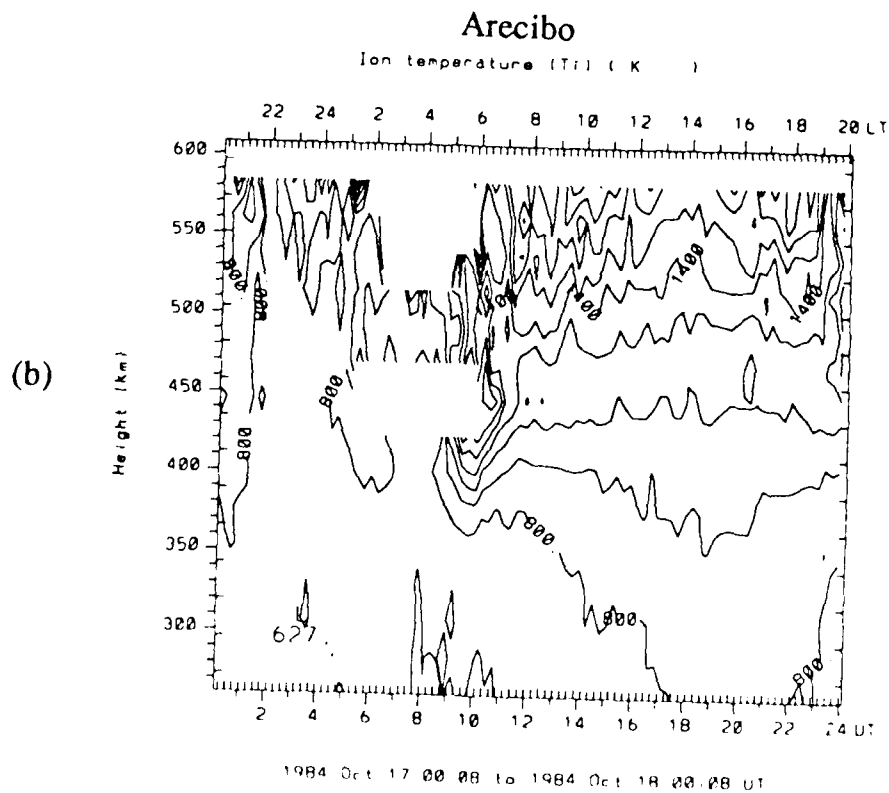
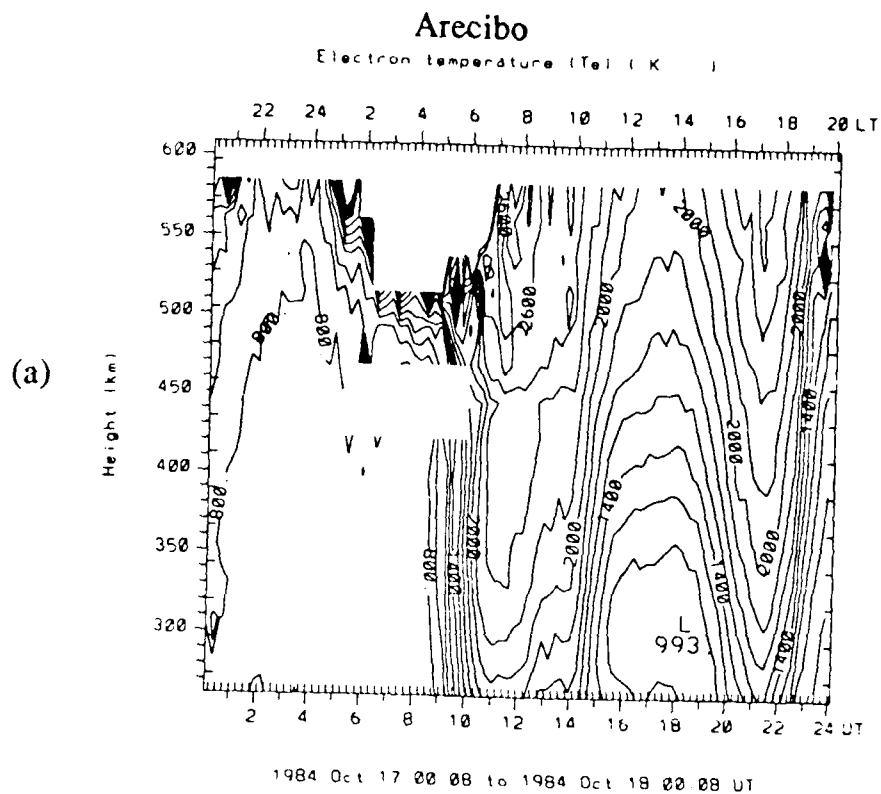
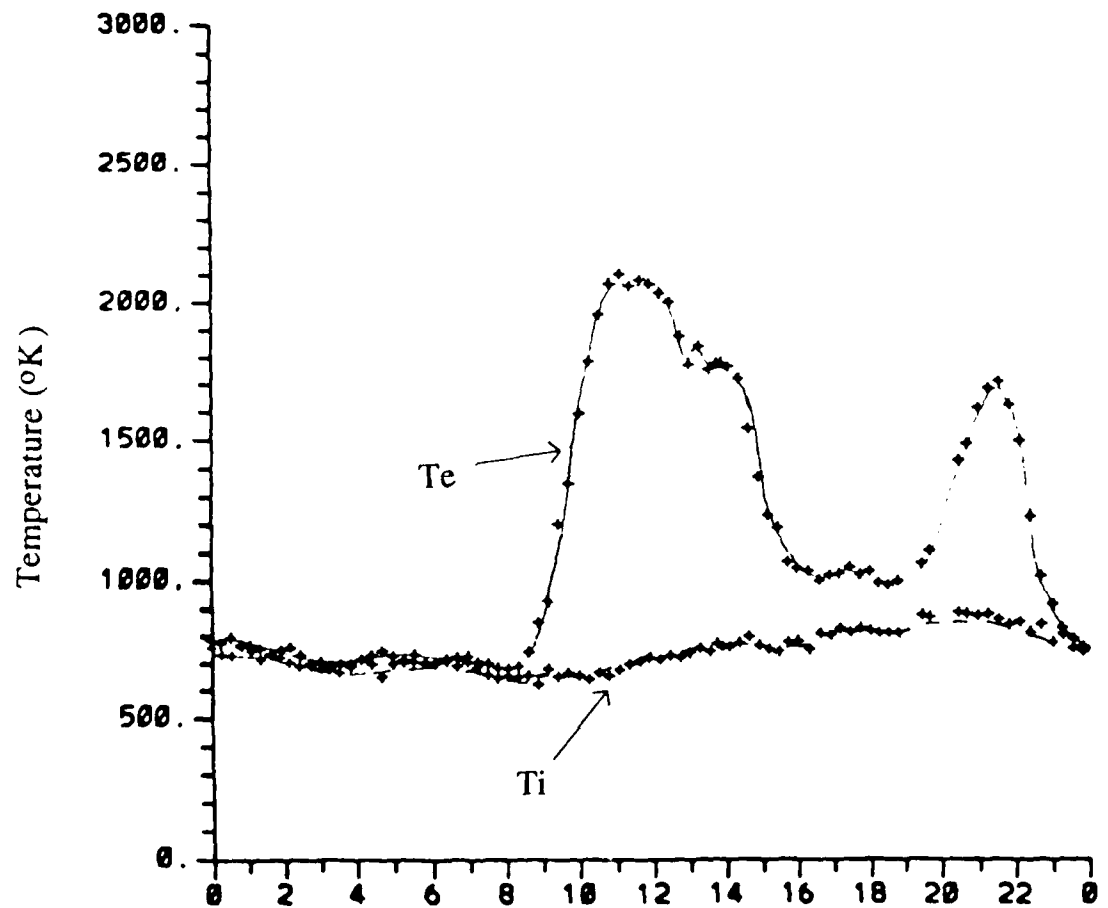


Figure 3-7

Arecibo Electron and Ion Temperature - 300 km



1984 Oct 17 00:00 to 1984 Oct 18 00:00 UT

UT = LT - 4

Figure 3-8

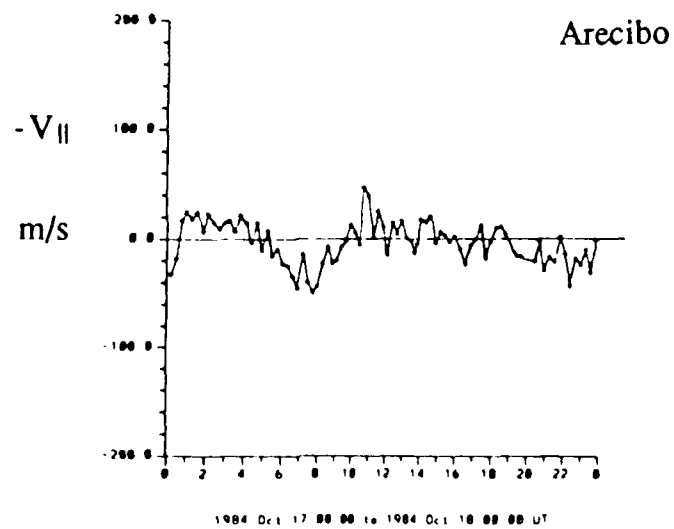
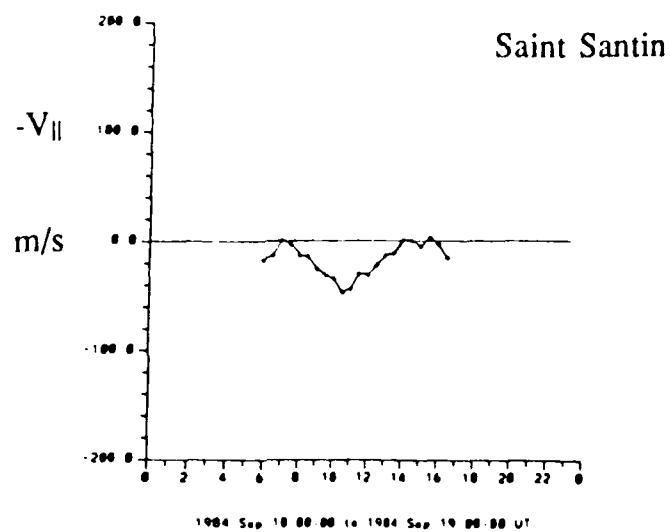
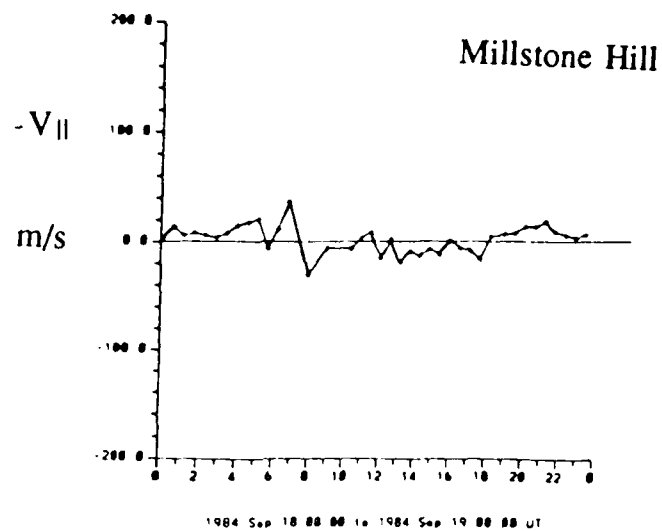


Figure 3-9

Chapter 4 The Disturbed Ionosphere:

The 19th of September 1984, was a disturbed day when a large magnetic storm commenced between approximately 0930-1000 UT (figure 4-1). There were two days of quiet geomagnetic conditions before the storm. This enabled the effects of the storm to be clearly seen in the ionosphere. The storm consisted of three substorms which comprised the overall disturbance, they occurred at 1000 UT, 1400 UT, and 1800 UT. During the substorms, large amounts of energy are input to the high-latitude ionosphere. This energy causes perturbations in the mid-latitude ionospheric parameters and will be discussed here. The quiet conditions discussed in chapter three will be referred to so that we can compare them with the storm affects in the topside ionosphere.

4-1 Millstone Hill Electron Density

By comparing the quiet diurnal variation in electron density (figure 3-1) with the disturbed day (figure 4-2) we see that there are significant differences in the two days. The electron density pattern does not exhibit just the diurnal growth and decay. There are perturbations on top of the diurnal cycle. These fluctuations are the ionospheric response to the energy being input at high latitudes. In particular, perturbations (indicated by arrows) can be seen at approximately 1200 UT, 1600 UT, and 2000 UT. The

perturbations correspond to the substorms commencement times with roughly a two hour lag time.

The time delay between the substorm commencements, indicated by the AE index, and the fluctuations in Ne implies that there is a propagation time from the auroral zones, where the energy is being input, to the ionosphere over Millstone Hill. Electric fields effects, from the auroral electrojets or the magnetosphere, occur instantaneously and can change the height of the ionosphere. Since there is a two hour time lag, this implies that the cause is of dynamical nature. When the energy is supplied to the high latitude ionosphere, a perturbation from Joule heating force is given to the neutral atmosphere and an equatorward wind is produced.

The entire topside ionosphere is raised on the disturbed day. Compare the log 10.7 per cubic meter electron density contour line in the quiet day (figure 3-1) and disturbed day (figure 4-2). This expansion of the ionosphere could be due to an increase heat input (see figure 4-3A), equatorward winds, or eastward electric fields.

The electron density on the disturbed day has also decreased. The maximum Ne is decreased by approximately 1×10^{11} per cubic meter on the storm day. This decrease defines the storm as a negative ionospheric storm. The exact cause of the decrease has not yet been determined because of the large numbers of parameters involved in determining

electron density such as latitude, time of storm onset, and intensity of the storm.

The diurnal pattern can still be seen in figure 4-2. The N_e increases between 0500-0600 LT with sunrise. The first N_e maximum occurs near noon and the second may be from the decrease in electron temperature causing a collapse of the ionosphere after sunset. The N_e then drops off rapidly after sunset and stays low throughout the evening.

4-2 Millstone Hill Electron and Ion Temperatures

The electron temperature on the storm day (figure 4-4) shows generally two major differences when compared to the 18th of September (figure 3-3, the control day).

Early on the 19th of September at 0200 LT, there is about a 400° K temperature rise. This is thought to have been caused by a particle precipitation event early before the major storm on September 19 began at 1000 UT.

The second difference is that there are higher electron temperatures at lower altitudes and higher temperatures persist for a longer time. The higher electron temperatures are mainly due to the decrease in electron density and thus a decrease in the ion content. The ions are the major cause of electron cooling and if the ion content decreased, the electron temperature will increase.

There is also a prominent temperature increase peaking at 1300 UT. It starts at 1000 UT which coincides with sunrise

and the commencement of the geomagnetic storm. The increase appears to be from the onset of the geomagnetic storm. After the increase at 1300 UT, the average T_e pattern shows smaller perturbations near 1600 and 2000 UT. These correspond with substorm related increases in electron density shown in figure 4-2. The average T_e is approximately 2200° K, this is about a 200° K increase over quiet time values on 18 September 1984 (see figures 3-3 and 4-4).

The ion temperature on 19 September also shows an increase occurring between 1300-1400 UT. The ion temperature after the peak is approximately 1000° K at 300 km. This is 50° K warmer than the ion temperature on the quiet day.

During 19 September, the electron temperature is always greater than the ion temperature. This is because of the increase of electron temperature occurring at 0200 LT.

4-3 Arecibo Electron Density

The electron density pattern at Arecibo on 19 September 1984 (figure 4-5) is very different than that on the quiet day (17 October 1984, figure 3-1). The height of the ionosphere is at a higher level on the disturbed day (compare the log 10.7 contour in figures 3-5 and 4-5). There is also a very prominent double-humped electron density structure. The first increase in N_e is due to sunrise and then by 1200 UT (0800 LT) equatorward winds from the storm induced circulation assist in raising the level of the ionosphere (figure 4-7A). This first

increase lasts until 1100 LT. The equatorward winds cease at 1100 LT and the level of the ionosphere decreases. This decrease in the level of the ionosphere has been given the name the midday bite-out. Rush et al. (1970) have attributed the bite-out to be caused by tidal effects. The diurnal and semi-diurnal tides are in opposition at the equator.

The second Ne increase is not as easily explained. There isn't a large increase in h_{\max} and there is no significant electric field or neutral wind observed. During a magnetic storm, Rush et al. (1969) have observed that the Equatorial anomaly is suppressed over the dip equator. After the storm it has been observed that the anomaly has a tendency to be more pronounced. This will give rise to diffusion of plasma towards Arecibo. The secondary maximum in electron density that's seen after the cessation of the storm (in the morning) could be due to this effect. When diffusion of ionospheric plasma takes place, the Ne increases (or crests) will be observed further poleward of the equator during storm times. This is evident here because on the quiet day, no anomaly features are seen in the Ne contour plots. The equatorial anomaly effects are usually seen within 20° North or South of the equator. Rush et al. (1969) have also indicated that the maximum development of the anomaly occurs locally at 1200 and 1600 LT. This is observed in figure 4-5 and indicates the anomaly has moved North to Arecibo (30° geomagnetic North).

The maximum electron density is lower on the 19th of September than the day prior. The 18th of September was not used as a control day because of a large data gap, but there was enough data gathered to determine that electron density decreased on the storm daily (figure 4-6).

The level of h_{\max} also exhibits a storm effect. At 2300 LT on 18 September, h_{\max} is at a maximum, which is then followed by a decrease corresponding to the post midnight collapse. This collapse, along with the h_{\max} variations due to the electric fields are discussed in chapter three up till sunrise. The quiet day description doesn't work with figure 4-7C after sunrise. A gradual increase in h_{\max} would be expected, but instead, a very large increase in h_{\max} is observed. Increases in h_{\max} come about from equatorward neutral winds or eastward electric field indicated by the perpendicular ion drifts (figure 4-7B). There are strong equatorward winds occurring over Arecibo when normally quiet-time winds would be poleward at this time.

4-4 Arecibo Electron and Ion Temperatures

The electron temperature starts to rise rapidly at sunrise (figure 4-9), but then decreases at 1330 UT, which is exactly when the electron density increases. The electron temperature is again inversely proportional to the electron density due to increased number of ion concentration which cools the electrons. The contoured shape in Figure 4-8A shows the same

shape as the electron density contours in Figure 4-5 until sunset when night time cooling, due to no solar photons, controls the T_e .

The ion temperature shows a diurnal variation. The T_i increases but only slightly compared to the control day.

4-5 Average Ionic Mass in the Topside Ionosphere

The types of ions that make up the ionosphere are important in determining electron density values since loss rates (recombination) are much greater if there are molecular ions present as opposed to atomic ions. During ionospheric storms, there can be an increase or decrease in the electron density (positive or negative ionospheric storms respectively). Generally speaking, a decrease in electron density is observed with a geomagnetic storm whether it is the day of the storm or the day after. This decrease in electron density has been attributed to an increase in the electron density loss coefficient due to increased molecular constituents. Prolss (1976) and Prolss and Von Zahn (1977) have made satellite observations of neutral composition in the thermosphere during geomagnetic storms and have been able to explain the negative storm from compositional changes.

The average ionic mass in the topside ionosphere should increase during geomagnetic storms if molecular constituents are increased. This can be determined from the slope of the

electron density profiles in the topside ionosphere. By using the definition of plasma scale height (H_p),

$$H_p = K(T_e + T_i) / \bar{M}_i g$$

the average ionic mass (\bar{M}_i) can be calculated. This is done by measuring the plasma scale height from the rate of electron density decrease in the topside ionosphere and by using observed electron and ion temperatures from the incoherent scatter radar. This was done at approximately hourly intervals for altitudes above the F2 peak up to around 600 km. An average "best-fit" slope was used to represent the decrease in electron density in the topside ionosphere. Average electron and ion temperatures were used for the calculated plasma scale heights. The results can be seen in Figure 4-10.

Equatorward winds would drive ionization up the field lines. Since the ionosphere is divided into molecular constituents below the F2 peak and atomic constituents above, an equatorward wind should increase the mean molecular ionic mass of the topside ionosphere.

The plot for Millstone Hill shows the mean molecular mass for the storm day deviating from quiet time values as early as 0700 UT. The equatorward winds from the storm don't arrive at Millstone Hill until 1100 UT. The increase in electron temperature before the onset of the geomagnetic storm plus the normally expected equatorward winds could be the cause of this early increase until 1400 UT. This is exactly

the time when the equatorward winds start to subside (see figure 4-11, top frame). After 1400 UT the mean ionic mass slowly approaches the quiet day values.

At Arecibo the equatorward winds are inferred from parallel ion velocities starting at 1200 UT (figure 4-11, bottom frame) and this is when the first major departure in mean ionic mass is observed. At 1500 UT the equatorward winds start to subside and the mean ionic mass is back to quiet time values by 1600 UT.

There are differences observed between the parallel ion velocity and mean molecular mass increases/decreases. These are due to the calculated mean ionic mass values only being every hour while the ion velocity measurements are made approximately every 15 minutes. The averaging of electron and ion temperatures must be taken into account. The fact that Arecibo's measurements seem to coincide better can be attributed to better height resolution of data observations at Arecibo (every 24 km) as opposed to Millstone Hill (every 48 km). The early increase in T_e (at 0200 LT) could be the cause of the increase in scale height which would increase the slope and thus the mean ionic mass before the start of the storm.

4-6 Parallel Ion Velocities

The radar has actually measured anti-parallel ion velocities. This just means the ion velocity upward along the magnetic field has been assigned positive values. During

geomagnetically quiet times, the parallel ion velocities are normally negative (downward motion, poleward wind) during the day and positive at night. This is due to the quiet time thermospheric wind circulation described in chapter one. Parallel ion velocities can also be due to electric fields (east or west) and diffusion velocity. The diffusion velocity is small near 300 km, the altitude which is plotted here, and can be ignored. The electric field's influence can only be verified at Arecibo since perpendicular ion drifts were unavailable for Millstone Hill and St. Santin. In Figure (4-11) the main perturbation in $-V_{\parallel}$ is the negative drop between 0800 and 1100 UT. The positive increases in $-V_{\parallel}$ between 1200 and 1600 UT indicate upward motion along field lines or equatorward winds. Since there is no or little perpendicular ion drift in figure 4-7C, the perturbation is due to equatorward winds in the morning hours when poleward winds would be expected for normally quiet times.

The inferred equatorward winds arrive at the radar stations at the following times:

Millstone Hill	1100 UT
St. Santin	1130 UT
Arecibo	1200 UT

The equatorward winds are due to the large heat input to the high latitude ionosphere. This heat is from Joule heating

from the auroral electrojet and/or particle precipitation from magnetospheric processes. Once the ionosphere is heated, heat is transferred to the neutral atmosphere and a buoyancy oscillation starts. This is the beginning of an equatorward (and poleward) traveling gravity wave.

Since the parallel ion velocities are known, meridional velocity component of the neutral wind can be calculated. Emery (1978) showed that the vertical ion velocity depended on plasma diffusion, electric fields, and on the neutral wind component parallel to the magnetic field. The diffusion velocity is small below 300 km and electric field effects are ignored, only for times when perpendicular ion drifts are small, so the meridional neutral wind would depend on the geometry of the magnetic field ($V_{\parallel}/\cos I$, where I = the inclination angle of the magnetic field). The magnetic inclination angle I , and geometric factors (which can be multiplied by the parallel ion velocities to get meridional neutral winds) for the radar sites are as follows:

	<u>Inclination Angle</u>	<u>Geometric Factor</u>
Millstone Hill	72°	3.2
St. Santin	63°	2.2
Arecibo	50°	1.6

This gives equatorward winds ranging from 115-160 m/s at Arecibo, 224-384 m/s at Millstone Hill, and velocities near

120 m/s at St. Santin. These values are in good agreement with observed Fabry-perot spectrometer results at Fritz Peak, Colorado (a mid-latitude station) Hernandez and Roble, 1978).

4-7 Global View of the Ionospheric Disturbance

Since the arrival time of the ionospheric disturbance is known at the three radar stations (time when strong equatorward winds are observed when normally poleward winds would be expected), a global view of the disturbance can be presented. To help present even a better picture of what's going on during this storm, data from the Assimilative Mapping of Ionospheric Electrodynamics (AMIE) procedure is presented. This procedure described by Richmond and Kamide (1988) uses several direct and indirect electrodynamic measurements and statistical patterns characterized according to solar activity level and latitude. This procedure gives us the best idea of how electrodynamic parameters are interacting (specifically Joule heating in this case).

By looking at figure 4-1, the storm starts between 0900 and 0930 UT. Since the times when the disturbance reached the radar sites and the commencement of the disturbance is known, an estimate of the propagation velocity of the disturbance can be made. Figure 4-12 shows the source of the propagation (from the Joule heating pattern) and the relative position of the radar sites. The disturbance takes from one to two hours to reach the radar locations so rotation of the earth

must be taken into account. After calculating great circle distances, a propagation speeds from 500-750 m/s are observed. These values assume constant propagation speeds, and don't take into account any deviation from the high-latitude circulation pattern that occurs from magnetospheric convection. Even with these assumptions, the values are in the range of the results obtained by several authors (for a good review, see Richmond and Roble, 1979).

Figure Captions for Chapter Four

Figure 4-1 Auroral electrojet magnetic indices from 0000 UT on 18 September to 0000 UT on 20 September 1984.

Figure 4-2 Diurnal variation of electron density over Millstone Hill on 19 September 1984. The height of maximum electron density is sketched as a dashed line.

Figure 4-3 Contours of diurnal variation of charged particle temperature over Millstone Hill on 19 September 1984. (a) electron temperature(T_e), (b) ion temperature (T_i)

Figure 4-4 Diurnal variation of electron and ion temperature at 300 km

Figure 4-5 Same as figure 4-2 for Arecibo.

Figure 4-6 Maximum electron density over Arecibo on 18-19 September 1984.

Figure 4-7 Diurnal variation of ion drifts and height of the F layer over Arecibo on 19 September 1984. (a) antiparallel ion velocity ($-V_{||}$), (b) perpendicular ion velocity in the northward direction ($V_{\perp N}$), (c) height of maximum electron density (h_{max}).

Figure 4-8 Same as figure 4-3 for Arecibo.

Figure 4-9 Same as figure 4-4 for Arecibo.

Figure 4-10 Average ionic mass of the topside ionosphere over Millstone Hill and Arecibo for quiet times (dashed lines) and disturbed conditions (solid lines).

Figure 4-11 Antiparallel ion velocities over Millstone Hill, Saint Santin, and Arecibo for geomagnetically disturbed conditions.

Figure 4-12 Polar cap view of Joule heating distribution from the Assimilative Mapping of Ionospheric Electrodynamics procedure. The relative locations of Millstone Hill (MLH), Saint Santin (STS), and Arecibo (ARO) are shown at the beginning of the storm. Their positions of the radars when the disturbance passes over head are also shown (MLH', STS', ARO').

AE Index for 18-19 September 1984

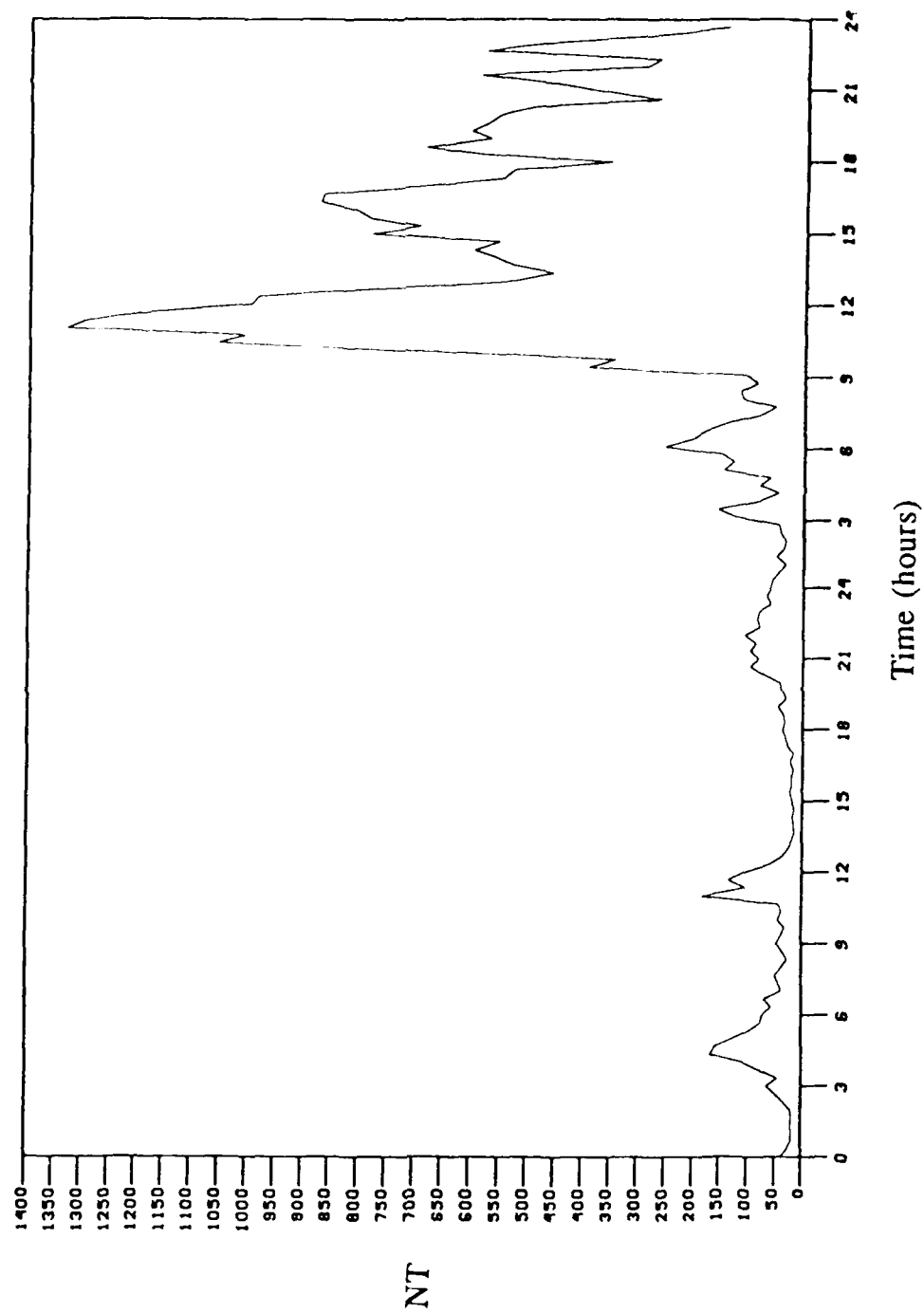


Figure 4-1

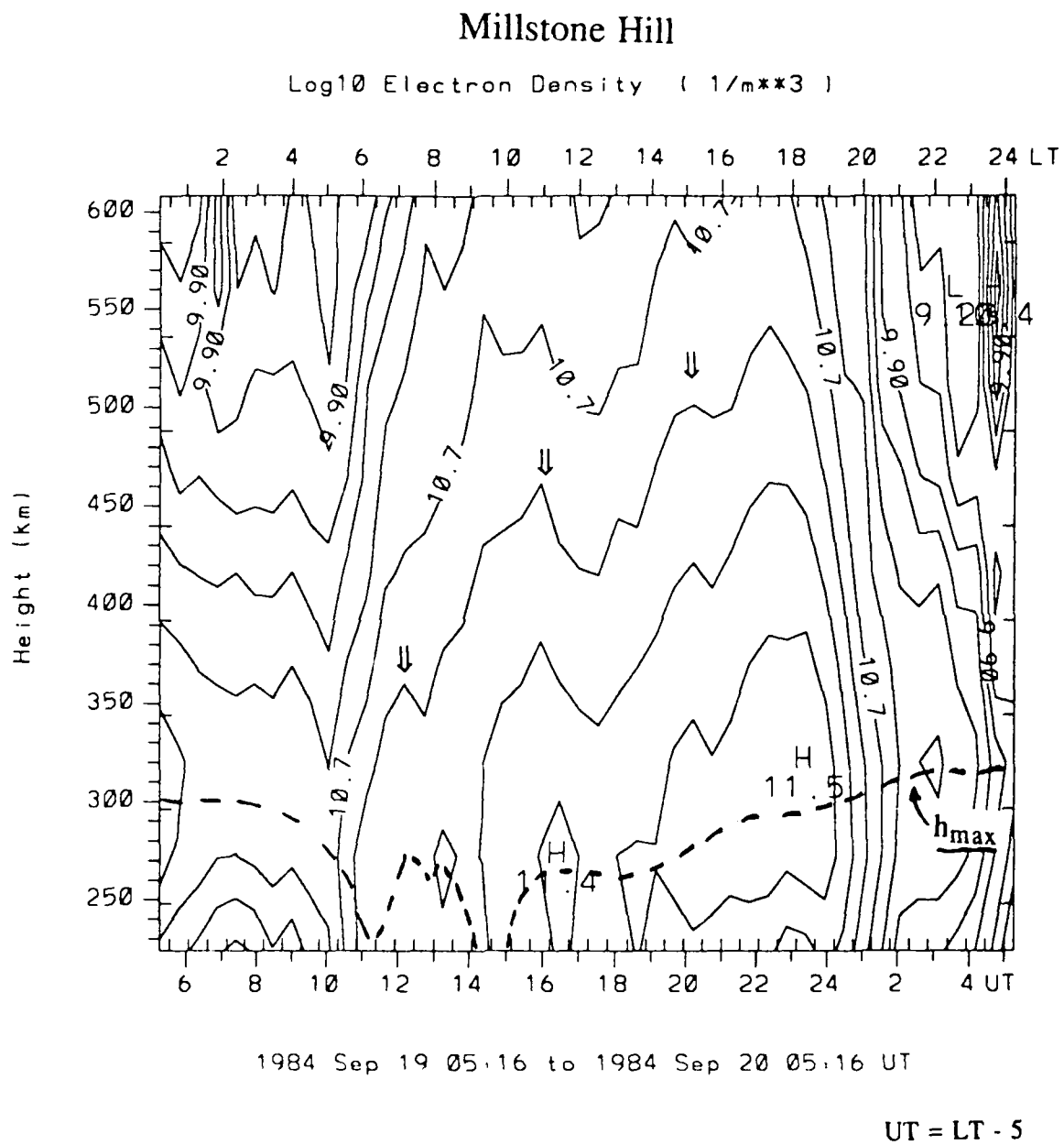


Figure 4-2

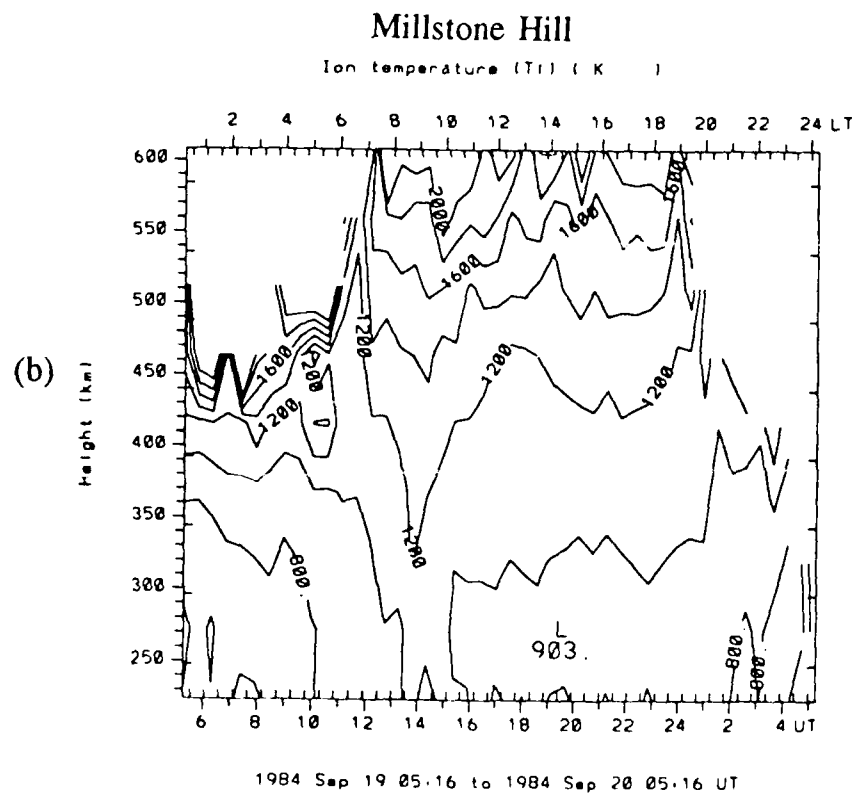
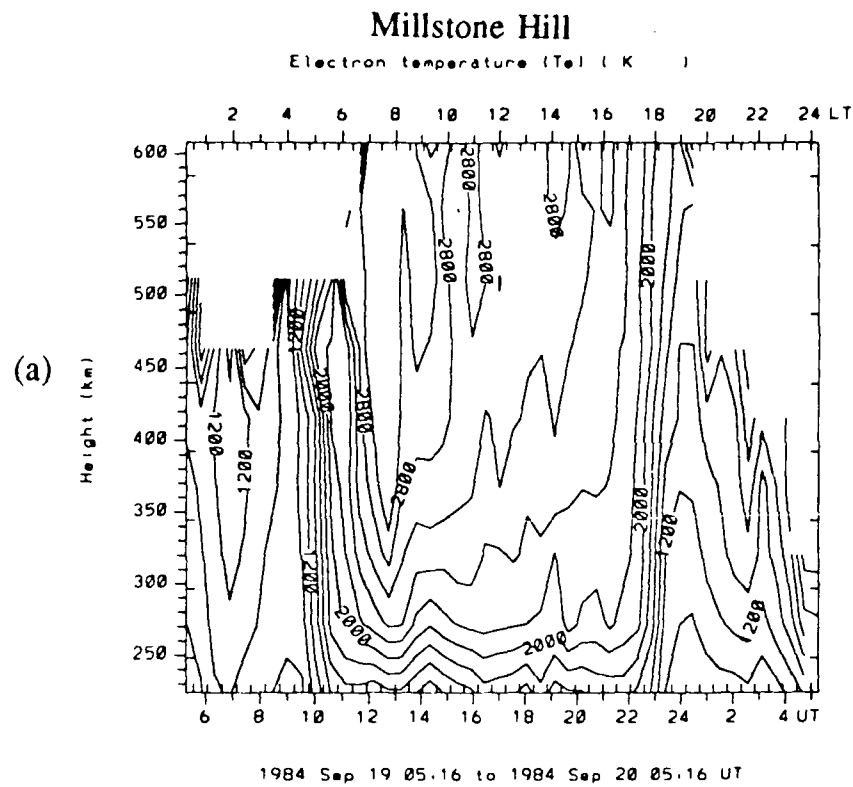
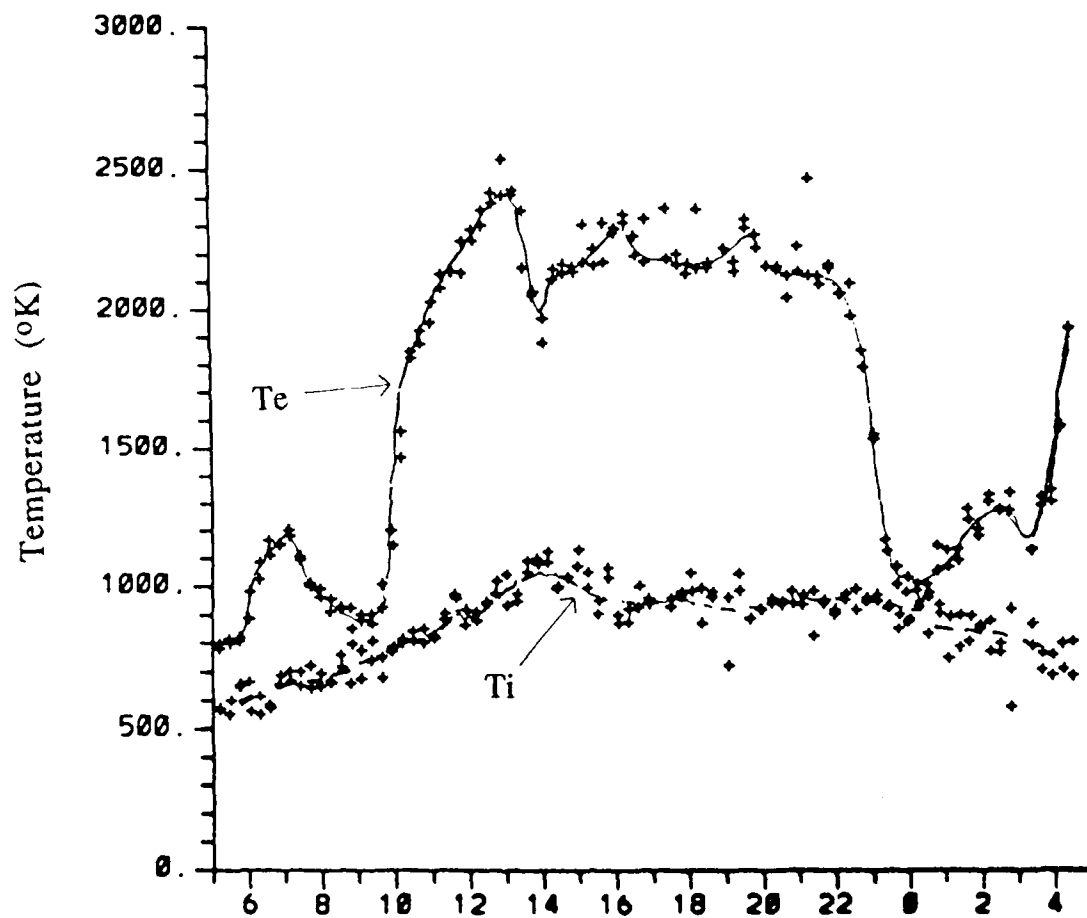


Figure 4-3

Millstone Hill Electron and Ion Temperature - 300 km



1984 Sep 19 05:00 to 1984 Sep 20 05:00 UT

UT = LT - 5

Figure 4-4

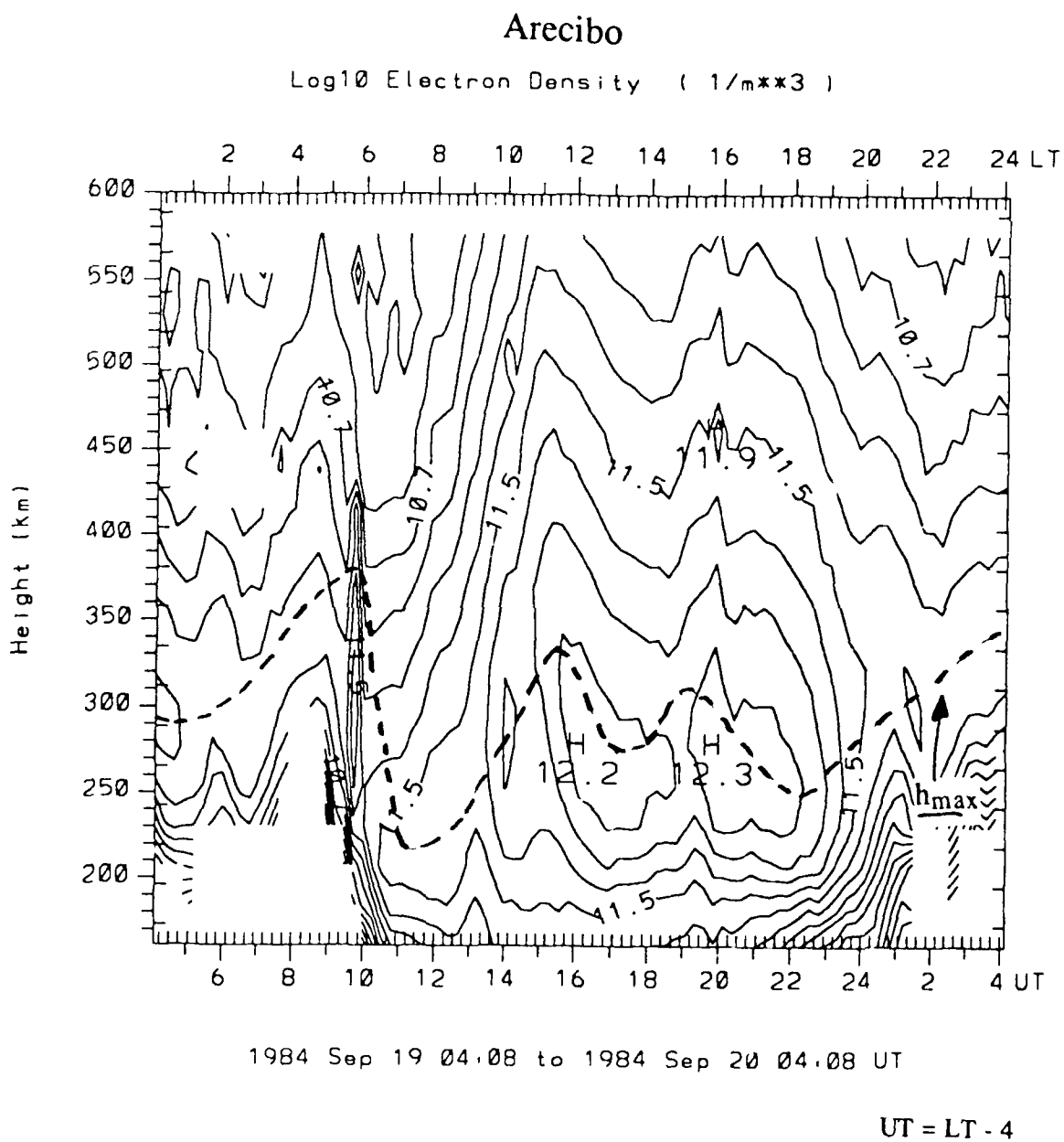
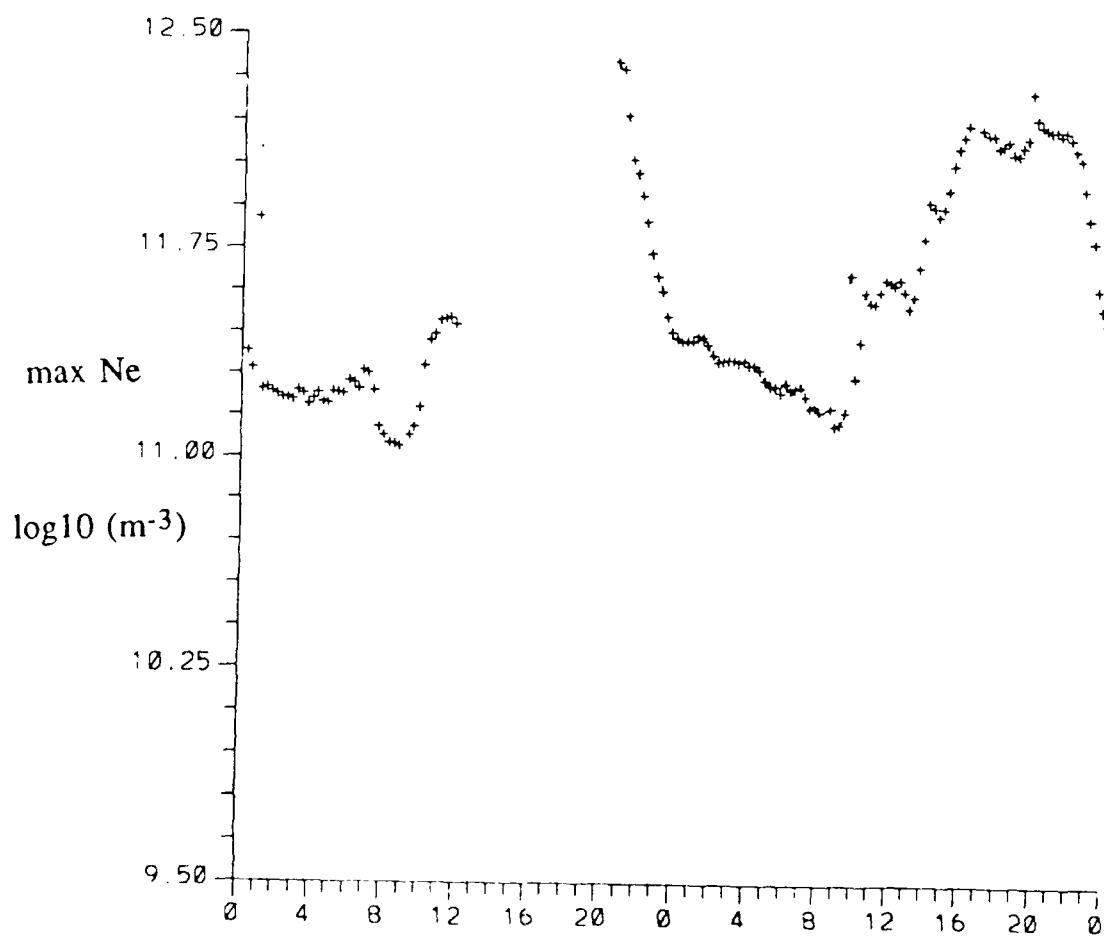


Figure 4-5

Maximum Electron Density at Arecibo



1984 Sep 18 00.00 to 1984 Sep 20 00.00 UT

UT = LT - 4

Figure 4-6

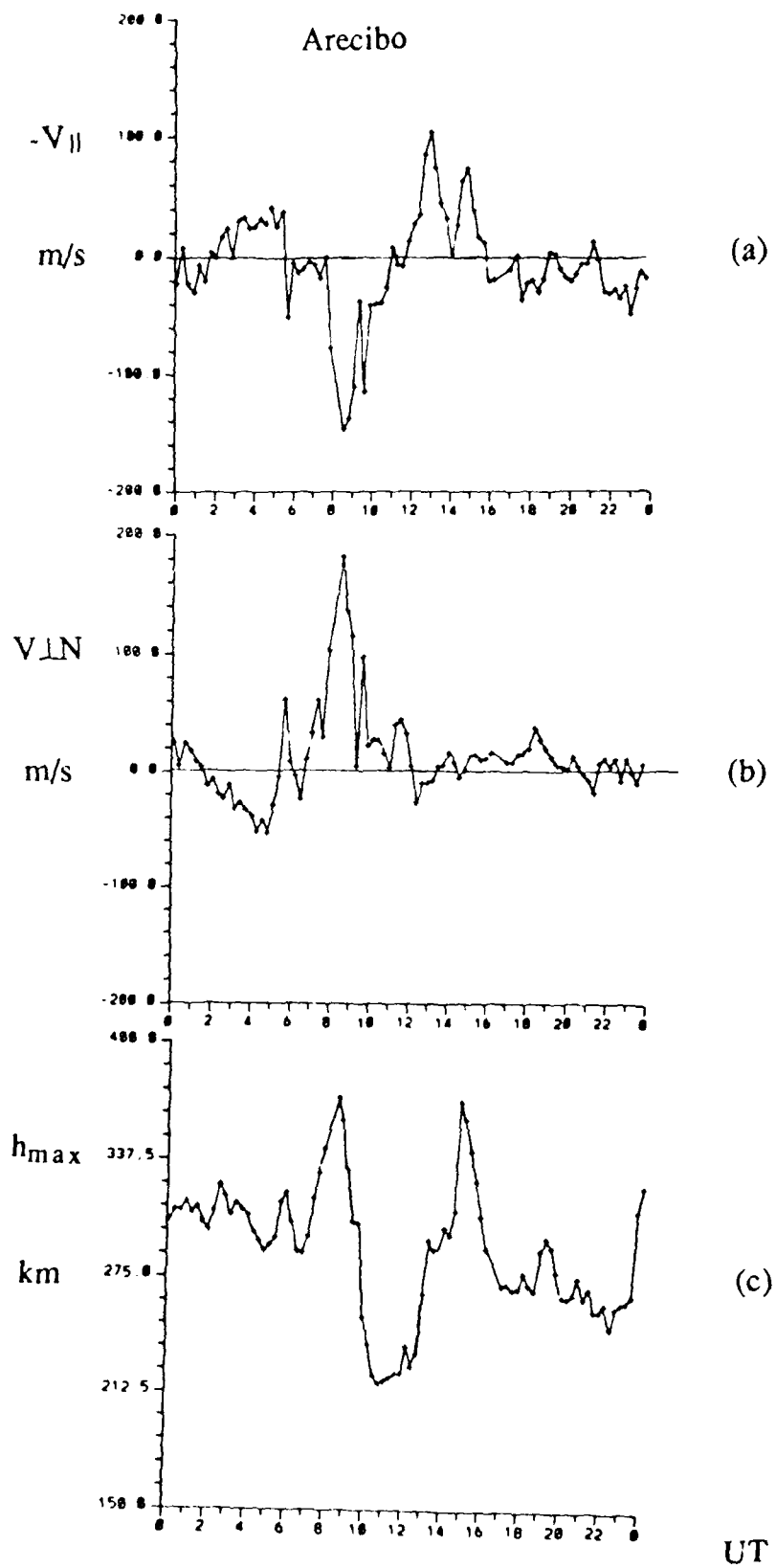


Figure 4-7

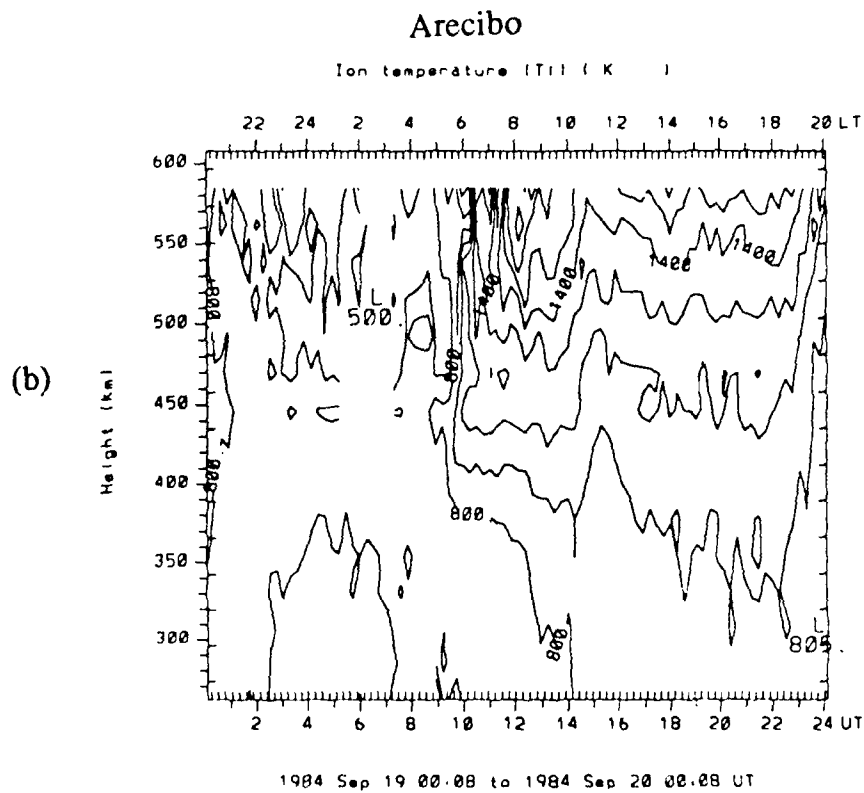
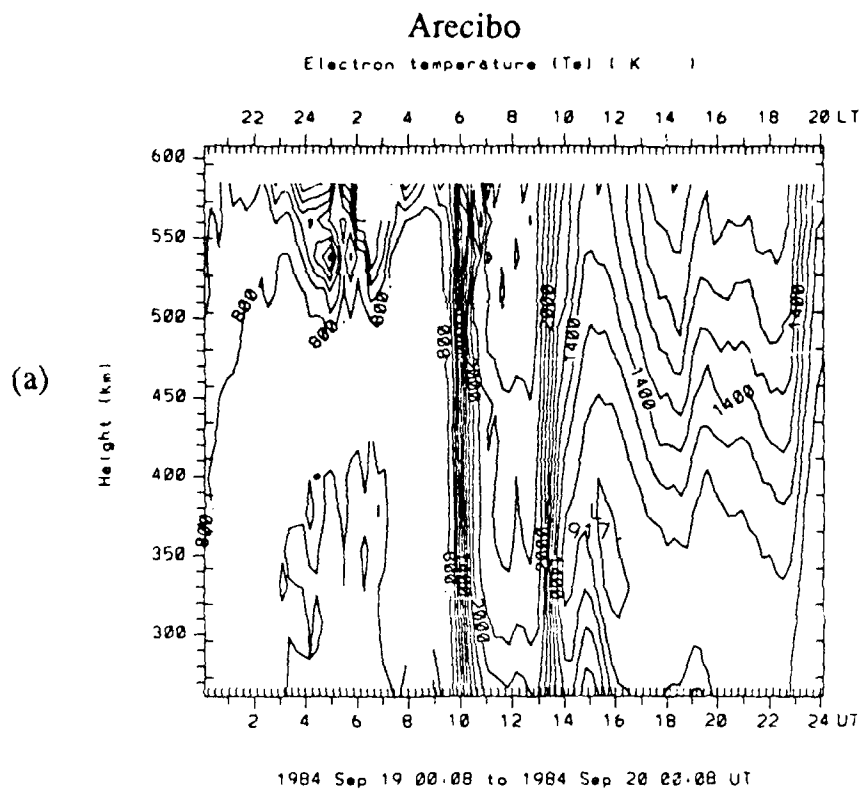
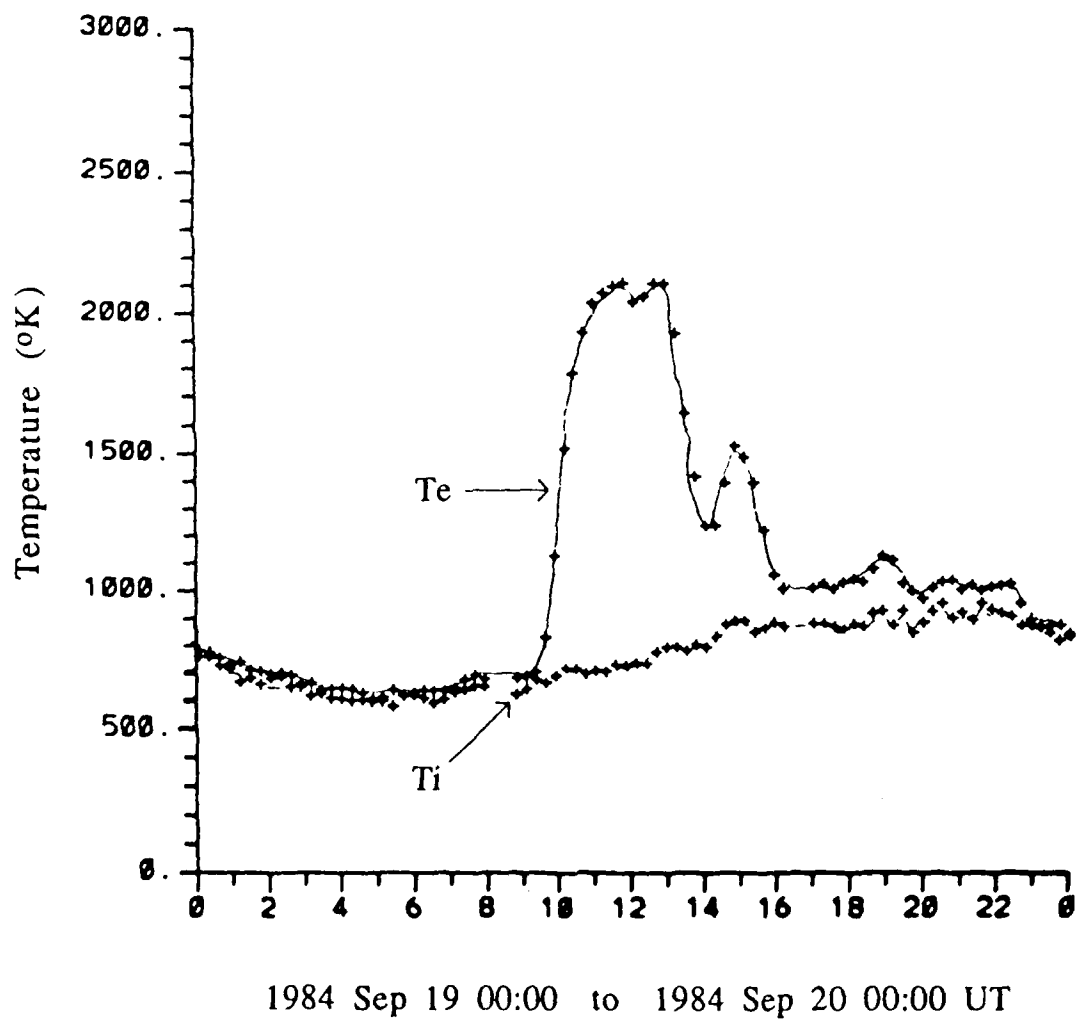


Figure 4-8

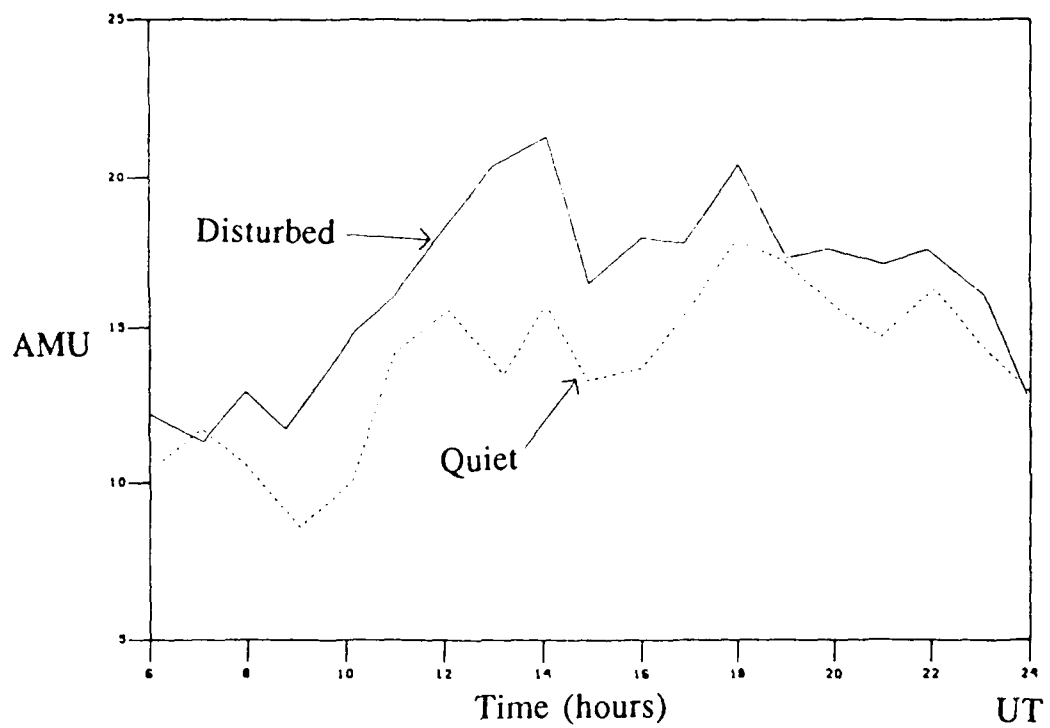
Arecibo Electron and Ion Temperature - 300 km



UT = LT - 4

Figure 4-9

Average Ionic Mass - Millstone Hill



Average Ionic Mass - Arecibo

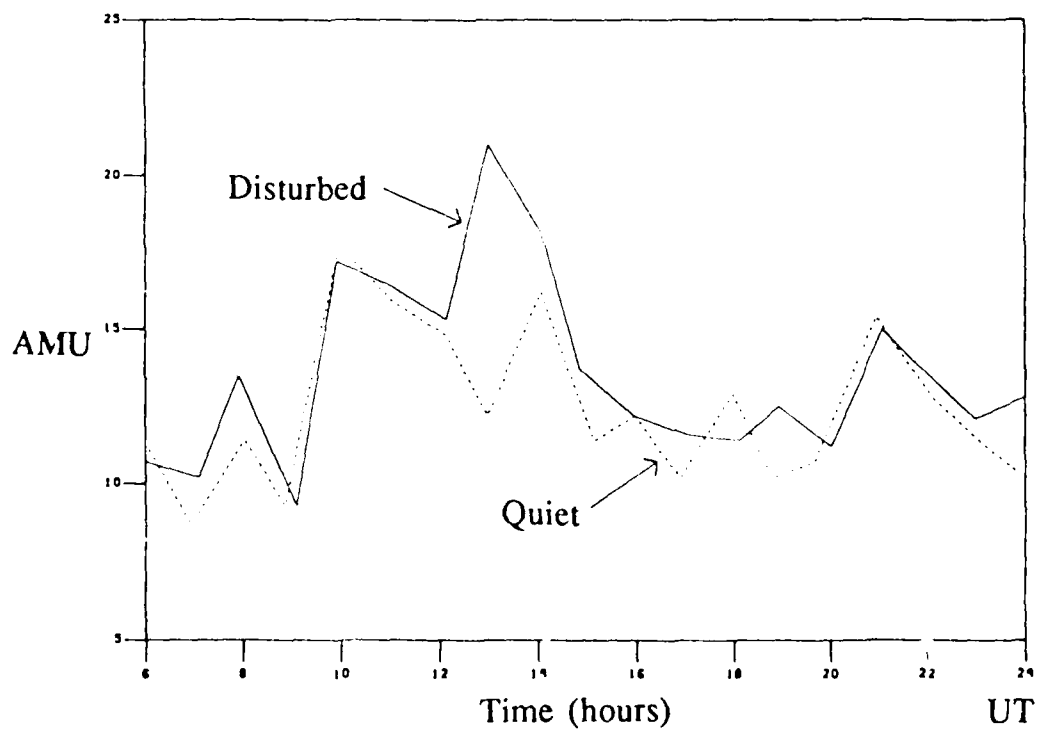
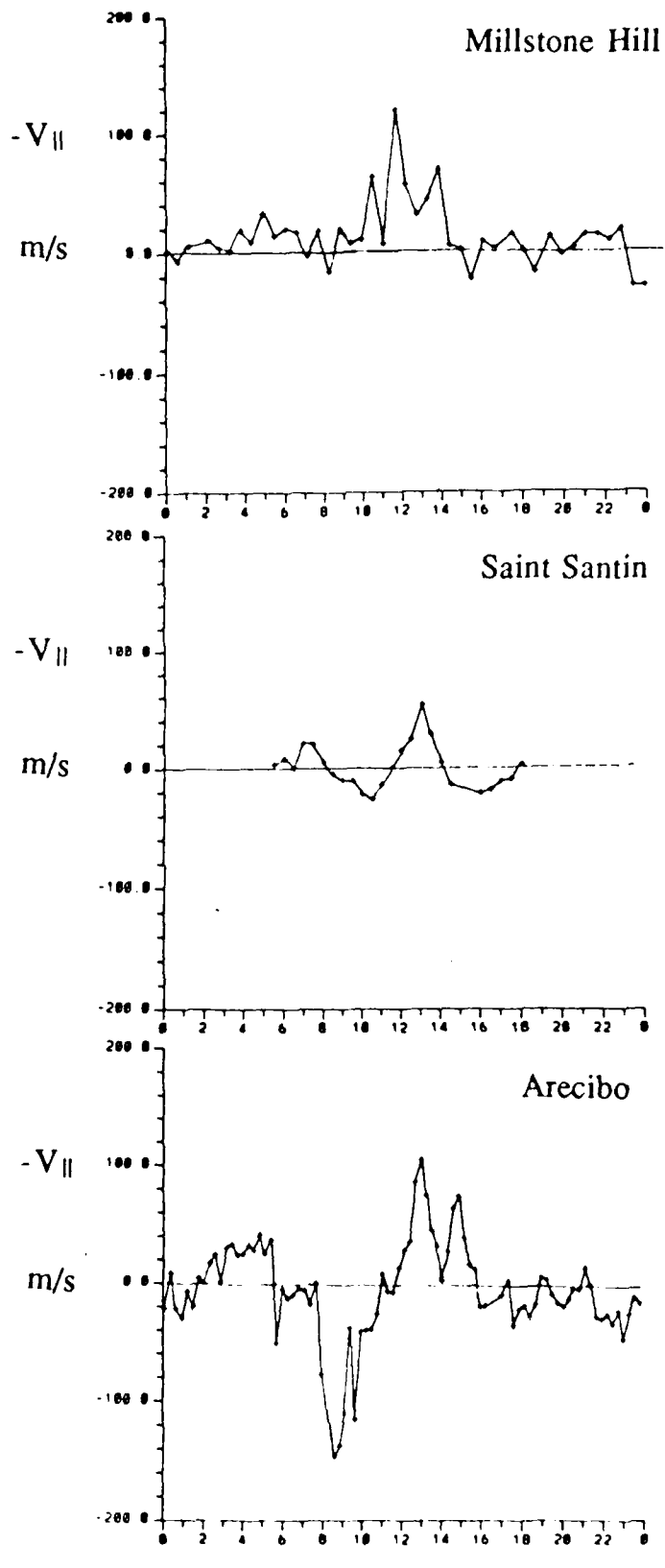


Figure 4 10



UT

Figure 4-11

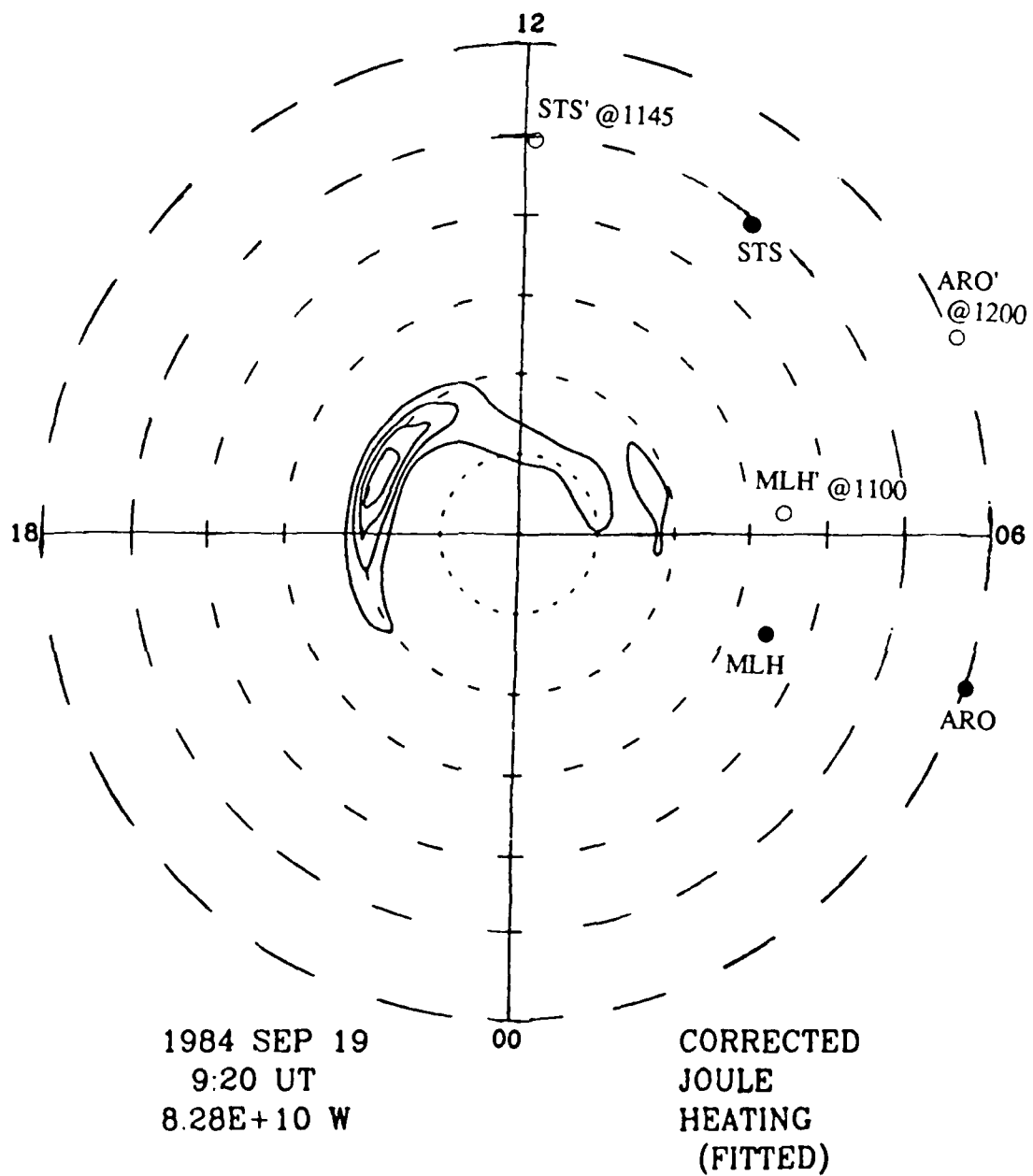


Figure 4-12

Chapter 5 Anti-Correlated Oscillations of Parallel and Perpendicular Ion Drift Velocities During a Geomagnetic Storm

The large scale variations in parallel and perpendicular ion drift components were looked at in chapter 4. In addition to the large scale variations, there are also small scale variations observed. Specifically variations in the parallel (V_{\parallel} measured positive up along the magnetic field line by convention of the incoherent scatter radar) and perpendicular ion drift velocity components in the magnetic meridian (V_{\perp}) are observed to be anti-correlated. This anti-correlation has been noticed by Behnke and Harper (1973), and is noticed to be more conspicuous in the nocturnal ionosphere.

There are three possible mechanisms that Walker (1980) reviews which are believed to be responsible for the anti-correlation. They are briefly described as follows:

Ion Drag - An eastward electric field will cause a northward perpendicular ion drift ($V_{\perp N}$). When $V_{\perp N}$ increases, collisions between the ions and neutrals also increases so that the neutral wind will gain a component in the poleward direction. This poleward wind will blow the ionization down the field line. In equilibrium, the ions and neutrals would move horizontally together. This mechanism provides an explanation for the anti-correlation between V_{\parallel} and $V_{\perp N}$. Ion drag works due to the ions colliding with the neutrals. There is

a problem because the time it would take for the ions to collide with all the neutrals at least once in order to drag the neutral atmosphere is too large in the nocturnal ionosphere when ion densities are low. It would take about an hour and a half to drag the neutral atmosphere and the response time between the ion drift components is much less than that (almost instantaneous).

Polarization Electric Field (or F Region Dynamo) - In this case, a poleward neutral wind creates an electric current perpendicular to the magnetic field. This is due to the neutral particle - ion collisions giving the ions a drift perpendicular while the electrons remain "tied" to the field lines. This current is carried by the ions and its direction is perpendicular to the force (the neutral wind) and the magnetic field (see Rishbeth and Garriott, 1969). A poleward wind will create a westward current. It's then supposed that conductivity irregularities inhibit the current flow and a polarization electric field is set up in the eastward direction. This polarization electric field causes an increase in $V_{\perp N}$ and that creates the necessary anti-correlation. The net motion is in the horizontal in the equilibrium state.

Diffusion Model - As in the ion drag mechanism, an eastward electric field causes an increase in $V_{\perp N}$. This raises the ionosphere to higher altitudes where the diffusion coefficient increases (because it is inversely proportional to the

collision frequency which decreases). Since the diffusion coefficient increases as altitude increases, there is an increase in the downwards diffusion velocity. This shows up in the data as an increase in the $V_{||}$ downwards when $V_{\perp N}$ increases. The net motion at equilibrium is once again horizontal.

Walker (1980) suggests that a test can be made to determine which mechanism is responsible for the anti-correlation of $V_{||}$ and $V_{\perp N}$. It depends on how h_{max} and the ion drift components vary. The responses are shown in figure 5-4. The ion drag mechanism initially has $V_{\perp N}$ increasing which raises the F layer. After the ions have collided with the neutrals for a long enough time to start the neutral atmosphere moving, a poleward wind develops which drives the ionization back down the field lines to its original height. The h_{max} and $V_{\perp N}$ would be positively correlated if the ion density were great enough to make the ion drift components fluctuate quick enough.

The level of h_{max} is predicted to decrease if the polarization electric field is the cause of the fluctuations. This is due to $V_{\perp N}$ being smaller than $V_{||}$. The $V_{\perp N}$ (from an eastward polarization electric field (E_p)) is the result of only part of the entire current flow. The electric current doesn't just stop at the conductivity irregularities, it must flow to somehow complete the circuit. Since only part of the current circuit causes E_p which creates $V_{\perp N}$, $V_{||}$ (down) is greater than $V_{\perp N}$ (up) and the F layer decreases.

In the case of the diffusion mechanism, the increase in $V_{\perp N}$ due to an eastward electric field causes the level of h_{max} to increase. The h_{max} will increase until diffusion velocity downwards achieves a new balance.

The important relationships to remember are that the diffusion mechanism provides a positive correlation between h_{max} and $V_{\perp N}$ while the polarization electric field gives a positive correlation between h_{max} and V_{\parallel} . The ion drag mechanism is discounted at night and the test is valid for the nocturnal ionosphere. It doesn't work during the day because the same positive correlation between h_{max} and $V_{\perp N}$ occurs for both ion drag and diffusion, thus no distinction can be made. The polarization electric field doesn't work by day either because any electric fields produced in the F region by day would be shorted out along the equipotential field lines into the highly conductive E region.

During geomagnetically quiet times the anti-correlation between V_{\parallel} and $V_{\perp N}$ can be seen in figure 5-5. The anti-correlation is observed during the day, but its more evident at night. To show that this is not an isolated case of the anti-correlation occurring more prominently at night, figure 5-6 shows another quiet case where the same conclusion can be made.

The level of h_{max} in figure 5-6 has a better positive correlation with V_{\parallel} than $V_{\perp N}$ during the night time periods. This would indicate that the polarization electric field is the

cause of the anti-correlation based on the test described above. Another example of this test in figure 5-7 shows a good positive correlation between h_{\max} and $V_{\perp N}$ from 0000 - 1100 UT. This time the diffusion mechanism appears to be responsible. The test between h_{\max}/V_{\parallel} or $h_{\max}/V_{\perp N}$ shows that both mechanisms, independently or each at a specific time of the night, can be responsible for the anti-correlation. Behnke et al. (1985) have shown cases where the cause of the anti-correlation can be attributed to diffusion in one case, polarization electric fields in another, and even one case where it seem neither mechanism fits. It's not intended to determine which mechanism causes the anti-correlation here, but to show how the anti-correlation varies during storms.

The anti-correlation of V_{\parallel} and $V_{\perp N}$ is shown for geomagnetically disturbed times in the figures below. In Figure 5-7 there are two prominent perturbation periods. The first exhibits an eastward electric field causing h_{\max} to rise while at the same time V_{\parallel} downwards increases.

The second perturbation period begins at 1200 UT (0800 LT, daytime). The level of h_{\max} rises significantly during this time and V_{\parallel} increases upwards. The perpendicular ion drift is small during this time, so the rise in h_{\max} is attributed to equatorward neutral winds. The increase in V_{\parallel} due to the equatorward neutral winds is at a time when downward V_{\parallel} would be expected due to diffusion velocity with h_{\max} increasing. There is probably downward diffusion occurring

but it's masked by the large upward $V_{||}$ from the neutral winds.

There are actually two perturbations caused by the neutral winds. During both of these perturbations there is anti-correlation with $V_{||}$ upwards and perpendicular ion drift in the southward direction ($V_{\perp S}$) which indicates a westward electric field.

Figure 5-8 shows another case where the anti-correlation is clearly seen during the day for a geomagnetically disturbed case. The data in figure 5-9 was obtained from the Saint Santin radar during a storm, and the prominent anti-correlation is again noticed during the day. This phenomenon is not peculiar to the ionosphere over Arecibo.

The anti-correlation in $V_{||}/V_{\perp}$ is seen to occur with stronger amplitudes during storm periods and also occurs more prominently during the day (if the equatorward winds from the storm arrive during the daytime hours). During quiet conditions, there's more of a tendency to have good anti-correlation at night when the height of the F layer is at higher altitudes. When storm-induced equatorward winds arrive during daytime, a situation similar to the nocturnal ionosphere is produced and good anti-correlation of $V_{||}/V_{\perp N}$ occurs during the daytime also.

Figure Captions for Chapter Five

Figure 5-1 Schematic representation of the ion drag mechanism. (from Walker, 1980)

Figure 5-2 Schematic representation of the polarization electric field mechanism. (from Walker, 1980)

Figure 5-3 Schematic representation of the diffusion mechanism. (from Walker, 1980)

Figure 5-4 Prediction of height of F layer and ion drift velocities for the three possible mechanisms. (from Walker, 1980)

Figure 5-5 Antiparallel ($-V_{\parallel}$) and the northward perpendicular ion drift ($V_{\perp N}$) measurements and height of the F layer over Arecibo on 17 October 1984.

Figure 5-6 Anti-correlation of V_{\parallel} and $V_{\perp N}$ over Arecibo on 14 September 1983.

Figure 5-7 Same as figure 5-5 for Arecibo on 19 September 1984.

Figure 5-8 Same as figure 5-6 for Arecibo on 2 November 1983.

Figure 5-9 Same as figure 5-6 for Saint Santin on 23 March 1979.

ION DRAG

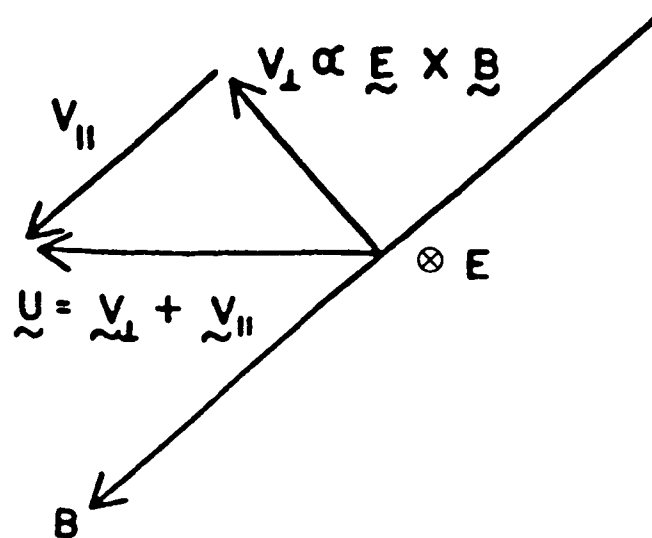


Figure 5-1

F-REGION POLARIZATION FIELD

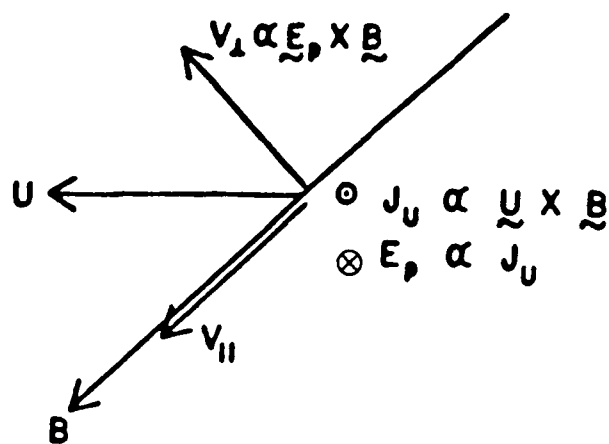


Figure 5-2

DIFFUSION

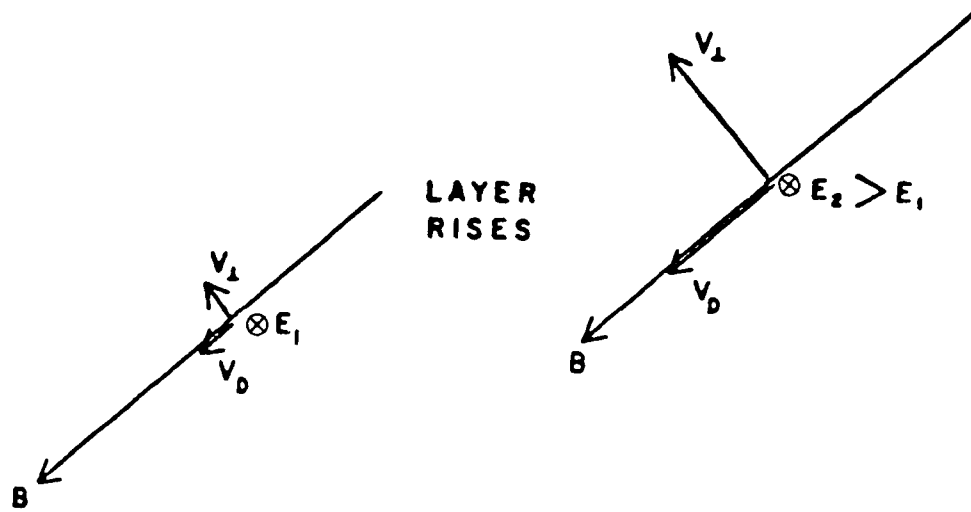


Figure 5-3

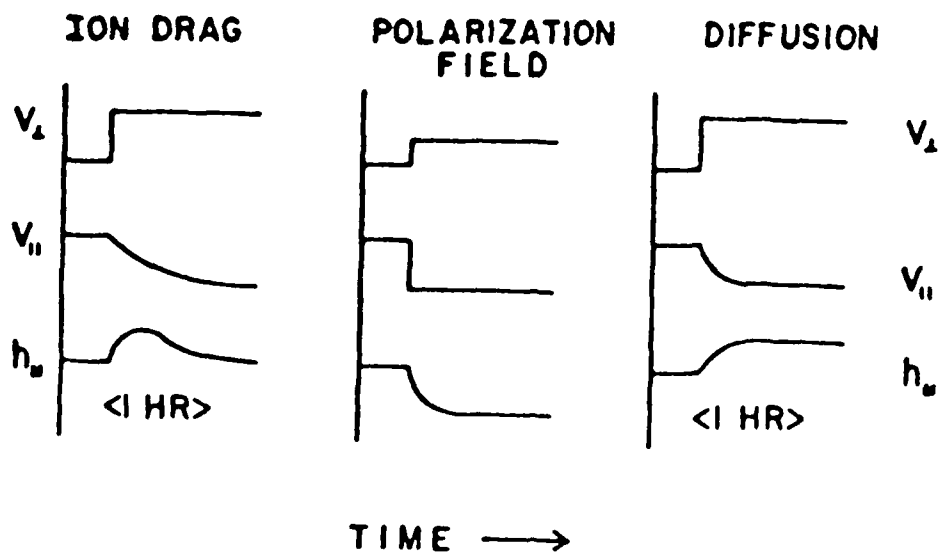


Figure 5-4

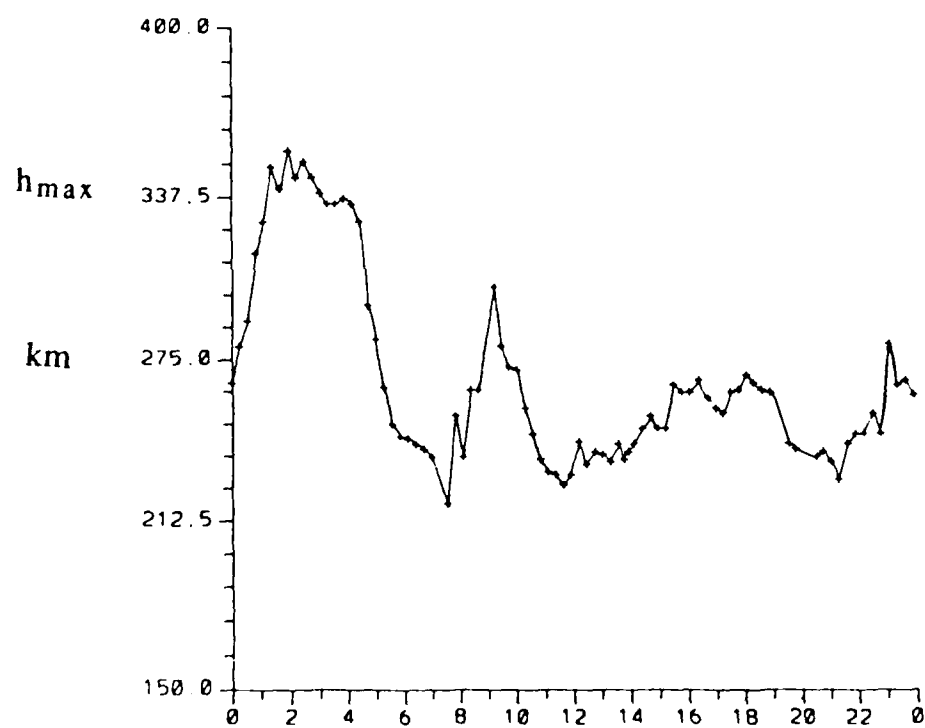
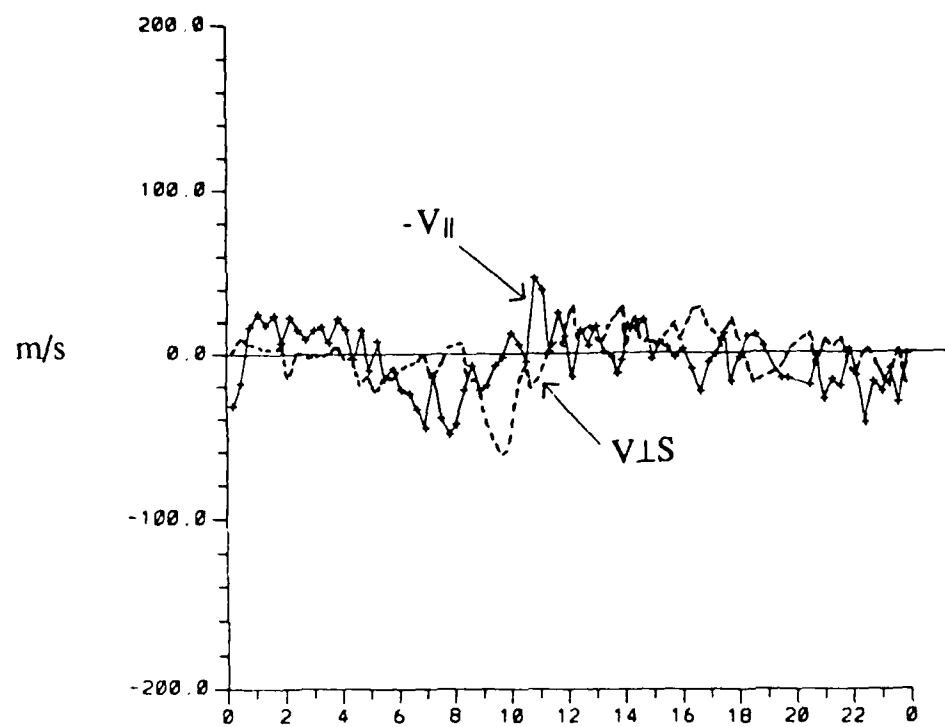
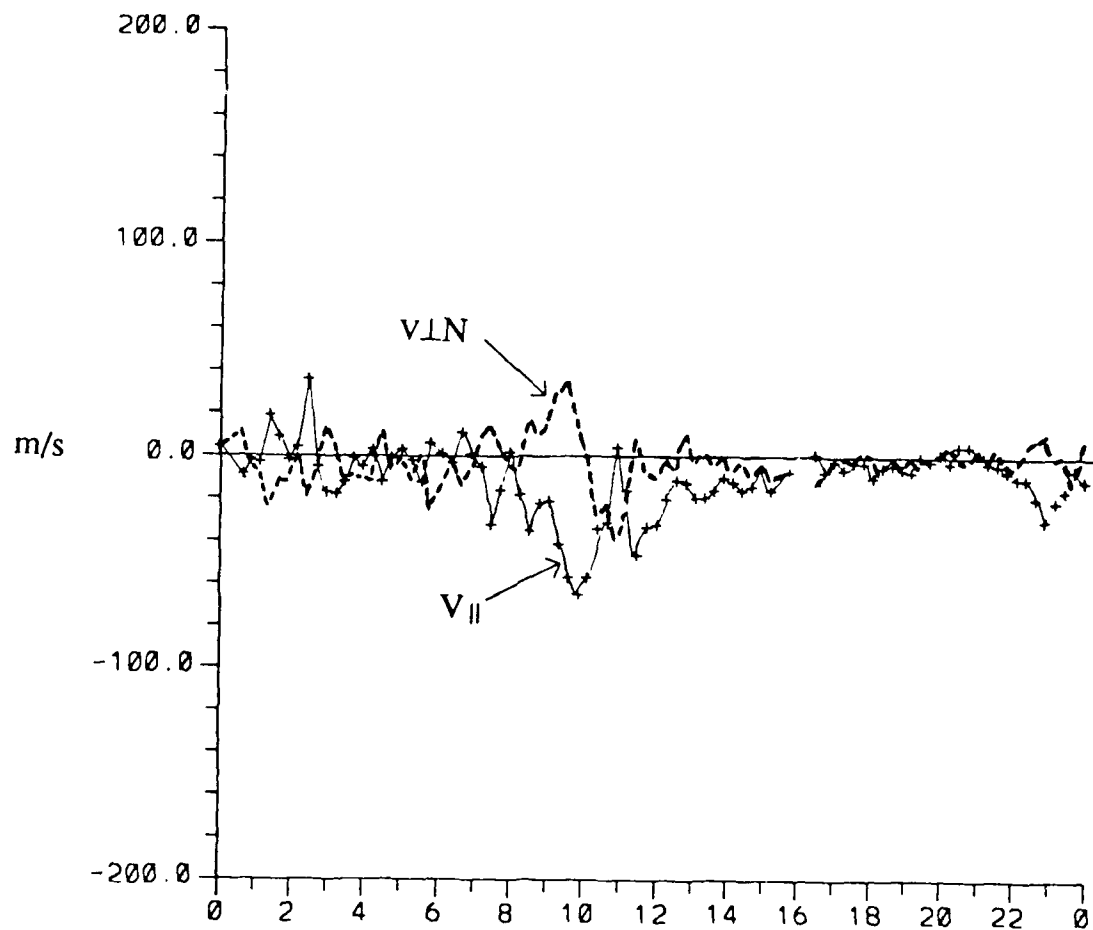


Figure 5-5

UT = LT - 4

Arecibo F Region Ion Velocity Components



1983 Sep 14 00:00 to 1983 Sep 15 00:00 UT

UT = LT - 4

Figure 5-6

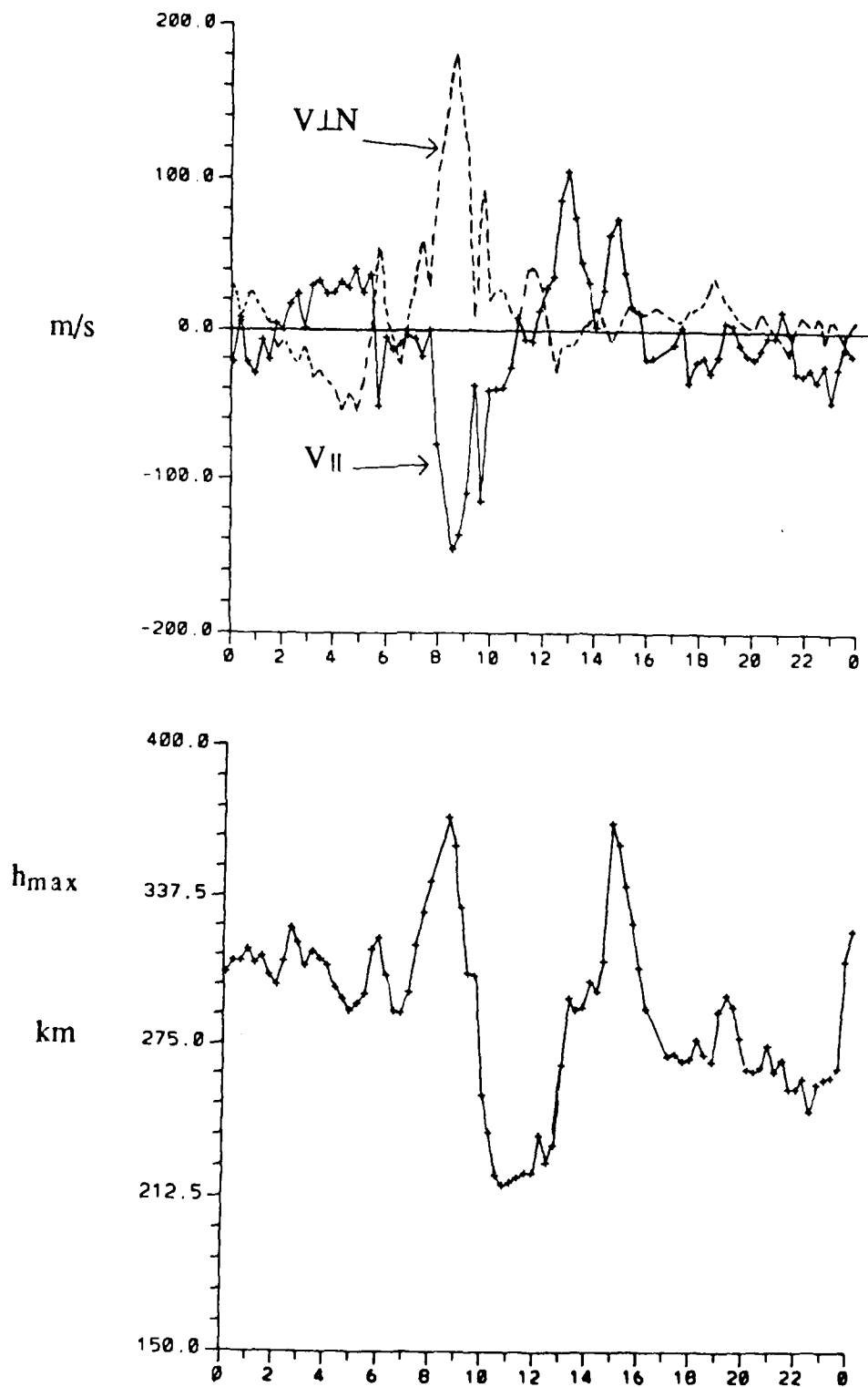
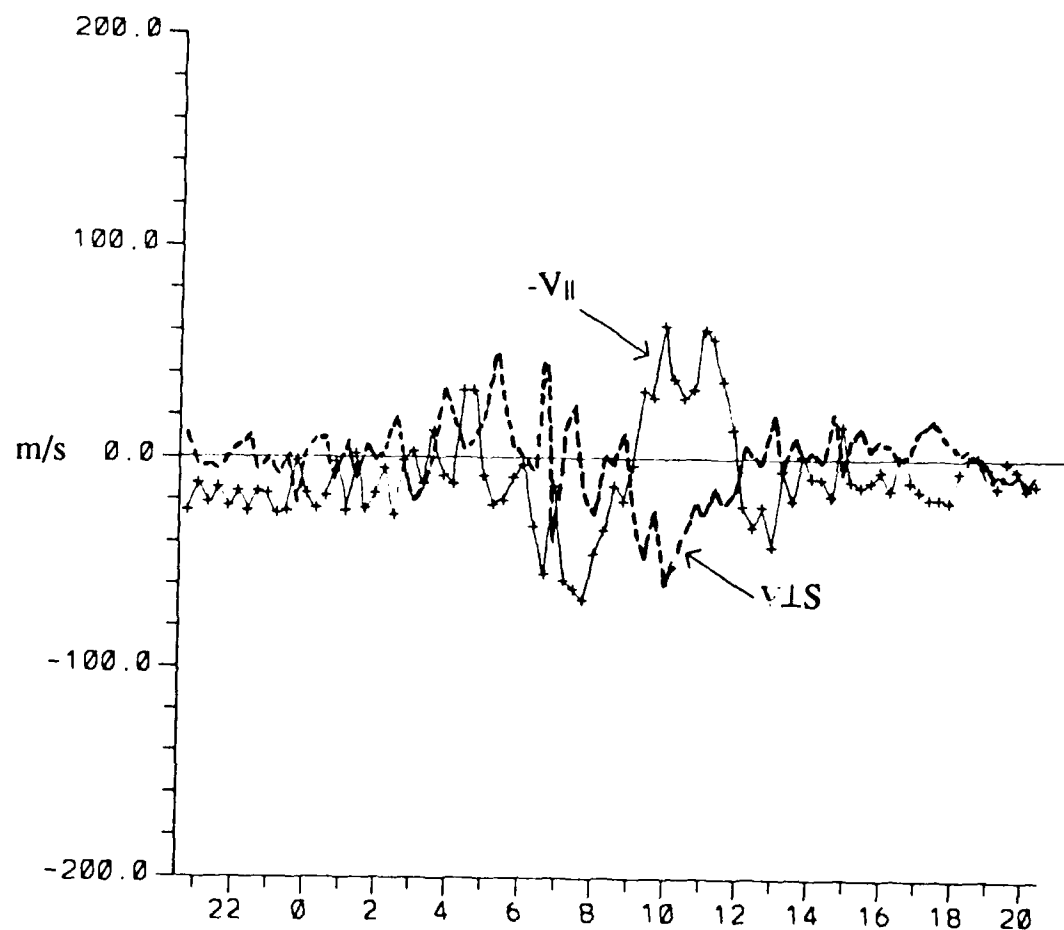


Figure 5-7

UT = LT - 4

Arecibo F Region Ion Velocity Components



1983 Nov 1 20:30 to 1983 Nov 2 20:30 UT

UT = LT - 4

Figure 5-8

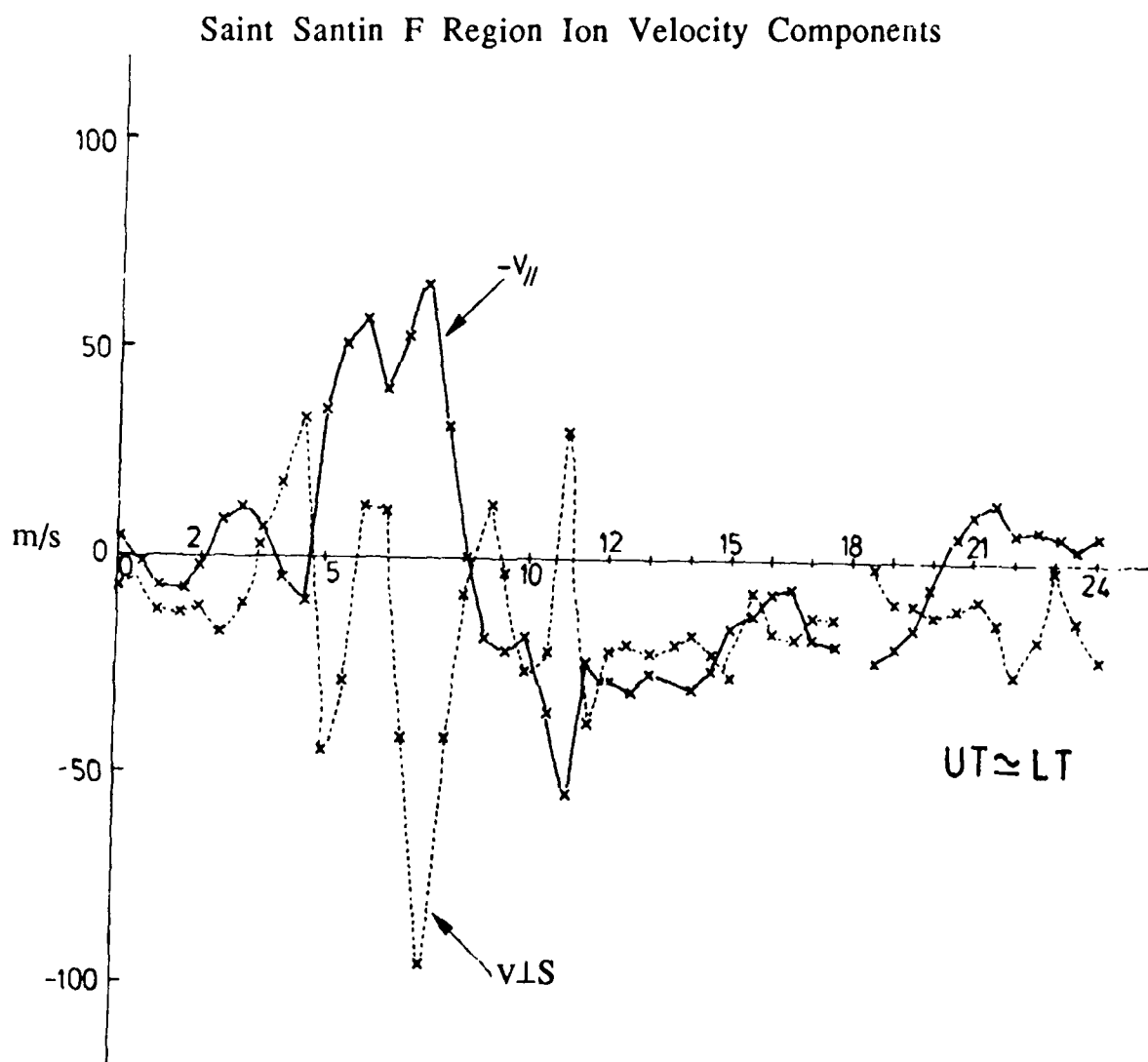


Figure 5-9

Chapter 6 Conclusions and Future Work

Ionospheric storms effects of the topside ionosphere have been observed at Millstone Hill, Saint Santin, and Arecibo. The main effect of the storm is an equatorward propagating disturbance in the neutral atmosphere which in turn affects the ionosphere as well. The main results from this study are as follows:

- 1) Perturbations in electron density are correlated with substorm commencement times with roughly a two hour time lag at Millstone Hill.

- 2) The electron density in the topside ionosphere is decreased on the storm day at Millstone Hill and Arecibo.

- 3) Electron temperature is higher and the duration of heating is greater on the storm day at Millstone Hill. There is also an electron heating event three hours before the commencement of the storm. There is no signature in the AE index of any magnetic substorm occurring, and since it occurs at 0200 LT it's likely that particle precipitation is the cause. There also appears to be electron temperature perturbations associated with the substorms that have the same two hour time lag as the electron density perturbations.

4) At Arecibo the electron temperature changes that occur are mainly due to changes in electron density. Arecibo is too far South to be influenced by particle precipitation events.

5) The average ionic mass in the topside ionosphere increases on the storm day. At Millstone Hill this increase occurs before the storm starts. This initial increase is due to the heating of the electron gas. This is because when the ionospheric plasma is heated, it expands and this expansion could cause the molecular portion of the ionosphere to be raised into the F region. A subsequent increase occurs due to the equatorward winds. When the equatorward winds start to subside, the average ionic mass approaches quiet time values. At Arecibo the increase in average ion mass corresponds very well with the equatorward wind disturbance.

6) Equatorward neutral winds induce parallel ion motion up the magnetic field lines. Perpendicular ion drifts correspond to electric fields and are found to be negligible. The equatorward wind disturbance is observed at the three radar sites; compare this to quiet conditions when poleward winds are expected. The equivalent meridional wind speeds calculated from $V_{||}/\cos I$ are in good agreement previous mid-latitude Fabry-Perot spectrometer observations during storm conditions.

7) The propagation speed of the disturbance was calculated by knowing where the disturbance started. It was possible to do this because the joule heating distribution from the AMIE procedure was available at the commencement of the storm. The propagation is seen to occur over the polar cap at velocities of 500-750 m/s.

8) It has been known from observations at Arecibo that there are anti-correlated oscillations between the parallel and northward perpendicular ion velocity components in the nocturnal F region. The present study shows that storm induced equatorward winds also produce these oscillations during the day. The polarization electric field mechanism wouldn't work during the day since the magnetic field lines are considered equipotentials and the lower E region has higher conductivity values.

Possible Areas of Future Work

- Calculate the ionic mass at higher height resolution to determine what ion types are pushed up the field lines and determine if this could be the cause for the negative phase of the ionospheric storm (decrease in electron density). Ionospheric parameters from the incoherent scatter radar can be input into models to determine diffusion rates or neutral composition changes in the F2 region.

- Use the entire incoherent scatter radar data base to analyze the anti-correlation of ion velocity components throughout the year (seasonal variation). By looking at a large number of cases, a statistical study could be done which could show which of the three possible mechanisms is responsible for the anti-correlation. Once the cause of the anti-correlation is known, there will be a better understanding of this feedback process and earth's ionosphere in general.

- A fourier analysis of the electron density perturbations can be made which could show how the periods of the waves change as height and distance away from the disturbance increases. This could lead to definite conclusions about gravity waves being produced from high latitude energy inputs.

REFERENCES

- Banks, P.M., and G. Kockarts, *Aeronomy*, Academic, New York, 1973
- Bauer, P., Theory of waves incoherently scattered, *Phil. Trans. R. Soc. Lond.*, **280**, 167, 1975
- Bauer, S.J., *Physics of Planetary Ionospheres*, Springer, New York, 1973
- Behnke, R.A., and R.M. Harper, Vector measurements of F region ion transport at Arecibo, *J. Geophys. Res.*, **78**, 8222, 1973
- Behnke, R.A., M. Kelly, C. Gonzales, and M. Larsen, Dynamics of the Arecibo ionosphere: A case study approach, *J. Geophys. Res.*, **90**, 4448, 1975
- Beynon, W.J.G., Incoherent scatter sounding of the ionosphere, *Contemp. Phys.*, **15**, 329, 1974
- Blanc, M., A.D. Richmond, The ionospheric disturbance dynamo, *J. Geophys. Res.*, **85**, 1669
- Chapman, S., The absorption and dissociative or ionizing effect of monochromatic radiation in an atmosphere on a rotating earth, *Proc. Phys. Soc. (London)*, **43**, 26, 1931
- Dickinson, R.E., and J.E. Geisler, Vertical motion field in the middle thermosphere from satellite drag densities, *Mon. Weather Rev.*, **96**, 606, 1969
- Emery, B.A., Neutral thermospheric winds deduced above Millstone Hill 1. Mathematical model, uncertainties, and representative results, *J. Geophys. Res.*, **83**, 5691, 1978
- Evans, J.V., Midlatitude F region densities and temperatures at sunspot minimum, *Planet. Space Sci.*, **15**, 1387, 1967
- Evans, J.V., Theory and practice of ionosphere by Thompson scatter radar, *Proc. IEEE*, **57**, 496, 1969

Evans, J.V., Some post-war developments in ground-based radiowave sounding of the ionosphere, *J. Atmos. Terr. Phys.*, **36**, 2183, 1974

Hargreaves, J.K., *The Upper Atmosphere and Solar Terrestrial Relations*, Van Nostrand and Reinhold Company, London, 1979

Hanson, W.B., and H.C. Carlson, The ionosphere, *The Upper Atmosphere and Magnetosphere*, National Academy of Sciences, Washington D.C., **84**, 1977

Harper, R.M., Nighttime meridional neutral winds near 350 km at low to mid-latitudes, *J. Atmos. Terr. Phys.*, **35**, 2023, 1973

Hernandez, G., and R.G. Roble, Observations of large-scale thermospheric waves during geomagnetic storms, *J. Geophys. Res.*, **83**, 5531, 1978

Jacchia, L.G., Static diffusion models of the upper atmosphere with empirical temperature profiles, *Smithsonian Contrib. Astro-Phys.*, **8**, 1965

Mazaudier, C., and P. Bauer, Nocturnal thermal disequilibrium of the F2 region ionosphere at middle latitudes, *J. Geophys. Res.*, **81**, 3447, 1976

Mazaudier, C., R. Bernard, and S.V. Venkateswaran, Saint Santin radar observations of lower thermospheric storms, *J. Geophys. Res.*, **90**, 2885, 1985

Moorcroft, D.R., On the determination of temperature and ionic composition by electron backscattering from the ionosphere and magnetosphere, *J. Geophys. Res.*, **69**, 955, 1964

Prolss, G.W., On explaining the negative phase of ionospheric storms, *Space Planet. Space Sci.*, **24**, 607, 1976

Prolss, G.W., and Von Zahn U., on the global morphology of negative ionospheric storms, *Space Res.*, **17**, 433, 1977

Ratcliffe, J.A., *An Introduction to the Ionosphere and Magnetosphere*, University Press, Cambridge, 1972

Richmond, A.D., and R.G. Roble, Dynamic effects of aurora-generated gravity waves on the mid-latitude ionosphere, *J. Atmos. Terr. Phys.*, **41**, 841, 1978

Richmond, A.D., and Y. Kamide, Mapping electrodynamic features of the high-latitude ionosphere from localized observations: Technique, *J. Geophys. Res.*, **93**, 5741, 1988

Rishbeth, H., and O.K. Garriot, *Introduction to Ionospheric Physics*, Academic, New York, 1969

Rishbeth, H., The F-layer dynamo, *Planet. Space Sci.*, **19**, 263, 1971

Rishbeth, H., F-region storms and thermospheric circulation, *J. Atmos. Terr. Phys.*, **37**, 1055, 1975

Roble, R.G., The calculated and observed diurnal variation of the ionosphere over Millstone Hill on March 23-24, 1970, *Planet. Space Sci.*, **23**, 1017, 1975

Roble, R.G., The thermosphere, *The Upper Atmosphere and Magnetosphere*, National Academy of Sciences, Washington D.C., 57, 1977

Rush, C.M., S.V. Rush, L.R. Lyons and S.V. Venkateswaran, Equatorial anomaly during a period of declining solar activity, *Radio Science*, **4**, 829, 1969

Rush, C.M., D.E. St. John, and S.V. Venkateswaran, A unified description of the tidal effects in f_oF_2 , *Radio Science*, **5**, 1413, 1970

Schunk, R.W., and A.F. Nagy, Electron temperatures in the F region of the ionosphere: Theory and observations, *Rev. Geophys. Space Phys.*, **16**, 355, 1978

Taieb, C., and P. Poinsard, Modelling of the mid-latitude ionosphere: Application to storm effects. II, *Ann. Geophys.*, **2**, 359, 1984

Walker, J., Correlation of wind and electric field in the nocturnal F region, *Geophys. J. R. Astron. Soc.*, **60**, 85, 1980